Design of FAIR low-energy cooler-buncher with simulations

Master's Thesis, 11.11.2021

Author:

Jouni Ruotsalainen

Supervisor:

Tommi Eronen

UNIVERSITY OF JYVÄSKYLÄ
DEPARTMENT OF PHYSICS

Abstract

Ruotsalainen, Jouni
Design of FAIR low-energy cooler-buncher with simulations
Master's thesis
Department of Physics, University of Jyväskylä, 2021, 87 pages.

A radiofrequency quadrupole cooler-buncher is a device used in low-energy ion beamlines, with the purpose of improving the quality of an ion beam. In this work, the geometry of the functional structure for such a device to be installed at the FAIR facility in Germany was designed using an ion trajectory simulation software SIMION. The goal of the simulations was to determine such a geometry and operational parameters that ion bunches of short temporal spread and small kinetic energy distribution could be created, while maintaining high transmission efficiency. In addition to finding optimal parameters, the effect of some key parameters on the bunch quality was assessed.

Using an incoming beam of singly charged ions with mass 100 u having 5 keV energy and 17 π·mm·mrad transverse emittance, a temporal width of 43 ns could be achieved, with a transmission of 96 %. The energy distribution of the bunch was 30 eV and the transverse emittance 9 π·mm·mrad with a kinetic energy of 5 keV. It was found that the gas pressure inside the device and the shape of the electric potential during the extraction of the bunch had the greatest effect on the bunch quality.

Compared to other RFQ cooler-bunchers currently in use, for example the JYFL cooler and the ISCOOL at ISOLDE, the achieved temporal spread was slightly lower and the transmission efficiency higher, while the energy spread was larger. As the simulated geometry was found to work well, the actual device can be constructed based on the model created in this work. With some adjustment, the optimised operational parameters obtained in this work can be used in the actual device.

Keywords: buncher, FAIR, ion beam, SIMION

Tiivistelmä

Jouni Ruotsalainen
FAIR-tutkimuslaitokseen tulevan ionikimputtimen suunnittelu ja simulaatio
Pro gradu -tutkielma
Fysiikan laitos, Jyväskylän yliopisto, 2021, 87 sivua

Ionikimputin on matalaenergisissä ionisuihkulinjoissa käytetty laite, jolla voidaan parantaa suihkun laatua. Tässä työssä suunniteltiin Saksan FAIR-tutkimuslaitokseen tulevan kimputtimen ionien liikkeeseen vaikuttavat osat hyödyntämällä ionien lentoratoja simuloivaa SIMION-ohjelmaa. Simulaatioiden tarkoituksena oli löytää kimputtimelle sellainen geometria ja käyttöparametrit, joilla voidaan tuottaa ajallisesti lyhyitä ionikimppuja, joissa myös ionien energiahajonta on pieni. Tämän lisäksi suihkun läpäisyn tulisi olla suuri. Lopuksi tarkasteltiin muutamien tärkeiden parametrien vaikutusta kimppujen laatuun.

Kimputtimeen syötettävällä suihkulla, joka koostui 100 u massaisista ioneista, joilla oli 5 keV liike-energiaa ja jolla oli 17 π·mm·mrad emittanssi, saatiin kimppuja, joiden lentoaikajakauma oli 43 ns ja energiajakauma 30 eV leveä. Suihkun läpimeno oli 96 %, emittanssi 9.0 π·mm·mrad ja ionien energia 5 keV. Simulaatioissa havaittiin, että suurin vaikutus kimppujen laatuun oli kimputtimen sisäisellä kaasun paineella ja kimpun laitteesta poistavan sähköisen potentiaalin muodolla.

Muihin tällä hetkellä käytössä oleviin kimputtimiin, esimerkiksi JYFL-kimputtimeen tai ISOLDEN ISCOOLiin, verrattuna saavutettu aikajakauma oli kapeampi ja läpimeno suurempi, joskin energiajakauma oli leveämpi. Simulaatioiden perusteella työssä suunniteltu geometria toimi hyvin ja laitetta voidaan alkaa rakentamaan. Työssä optimoituja käyttöparametreja voi pienten sovitusten jälkeen hyödyntää varsinaisessa laitteessa.

Avainsanat: Kimputin, FAIR, ionisuihku, SIMION

Contents

1 Introduction

A radiofrequency quadrupole (RFQ) cooler-buncher is a device used in radioactive ion beam research facilities to allow for more accurate measurements on nuclear properties. Some of the applications that benefit from the use of a buncher the most include collinear laser spectroscopy and nuclear decay studies by reducing the background noise [1–3], and Penning trap mass spectrometry [4, 5].

In order to study the properties of radioactive nuclei, they need to be produced in nuclear reactions, as most are not found in nature due to their short half lives [6]. The ionised reaction products are then transported to the experimental setup as a beam of ions, in which the stream of individual ions move in the same direction with velocities much higher than a particle at room temperature. Due to the violent nature of the nuclei production methods, the ions receive a range of kinetic energies and slightly different directions, typically resulting in an ion beam of poor quality [1, 7]. Moreover, the ions are often produced in a continuous stream. As these characteristics often play a large role in the accuracy and usability of many measurements, the RFQ cooler-buncher, known also as just the buncher, can be used to make the beam better suited to a particular experiment [8–11]. This is achieved by cooling and optionally bunching the ion beam.

To operate the buncher, the ion beam is injected into the device. With the use of static and alternating electric fields and a low-pressure gas, the fast moving ion beam is thermalised, known as cooling, reducing the size of the beam and the energy spread of the ions [8–10]. To bunch the beam, the ions can be stored in the buncher for a short while, releasing the accumulated ions as ion bunches. The cooled ions in a bunch then have similar energies and directions, and thus the buncher can be thought to reset the beam quality, so that the extracted beam characteristics depend only on the buncher itself.

At the time of writing (autumn 2021), a new research facility named the Facility for Antiproton and Ion Research in Europe (FAIR) is being constructed in Darmstadt, Germany [12, 13]. In this work, the geometry for a buncher to be placed into a low energy branch of the facility was designed and its performance evaluated using

simulations. In addition to designing the buncher consisting of a main section and a two bunching sections, the injection and extraction optics required to get the ions in and out of the device efficiently were also designed. In the design, only the functional parts manipulating the motion of the ions are included, meaning that all the supporting structure keeping these parts in place were left out of this work.

The design was created using a 3D modelling software Autodesk Inventor, and the simulations were done using an ion trajectory simulation program SIMION. Integral to the design process was using the simulations to optimise the operational parameters of the buncher, such as the gas pressure and voltages applied to the various parts, so that good quality bunches could be obtained. In the simulations, the incoming beam was assumed to have certain characteristics and the goal was to create ion bunches with short temporal spread and small energy distribution, while maintaining fast operation and high transmission efficiency. In the design, a novel method of creating the DC electric potential transporting the beam through the buncher is implemented.

In this thesis, first the operation of radioactive ion beam facilities is touched upon, followed by a consideration of the various phenomena regarding ion beam transport relevant to bunchers. Then the structure and operation of a typical buncher, and the software used in this work are presented. Finally, the buncher designed in this work is introduced, along with the many simulations assessing the performance.

2 Background

Studying the fundamental properties of atomic nuclei has many applications in a multitude of research fields beyond nuclear physics itself, including (nuclear) astrophysics [14], material physics and medicine [13]. As most exotic nuclei being studied are radioactive, they must be produced and transported to the measurement device before they decay.

Due to the cost of operating the equipment needed for nuclear research, large facilities housing multiple research groups sharing much of the equipment have become commonplace. At the heart of such a facility is the production site of the nuclei, commonly utilising particle accelerators to fuse and smash nuclei to produce the exotic nuclei of interest. As the production site is too radioactive to perform accurate measurements, the ionised reaction products are formed into an ion beam and transported to the measurement device further away. These transport lines are commonly called beamlines. Unfortunately, the beams obtained from an ion source are often of poor quality, leading to a lot of wasted nuclei [8–10]. In many nuclear research facilities, a radiofrequency quadrupole (RFQ) cooler-buncher is used to improve the quality of the beam and make it suitable for the experimental setups downstream. Examples of such facilities are the upcoming FAIR facility in Germany and the IGISOL facility at University of Jyväskylä, presented in figure 1.

2.1 FAIR

At the low energy branch of the FAIR facility at GSI, the nuclei to be studied are produced with the in-flight method [13]. In the method, a thin target of some light material, such as nickel, is bombarded with a beam of high energy (>100 MeV/u) heavy ions, such as uranium. The colliding heavy ions then disintegrate to exotic, somewhat lighter than target nuclei that recoil out of the target as ions. The ions of interest are then separated using the super fragment separator [7] and captured in a cryogenic stopping cell [15]. In the cell, the ions are slowed down and extracted as low energy (∼10 keV) ion beam. This method produces a wide beam with the

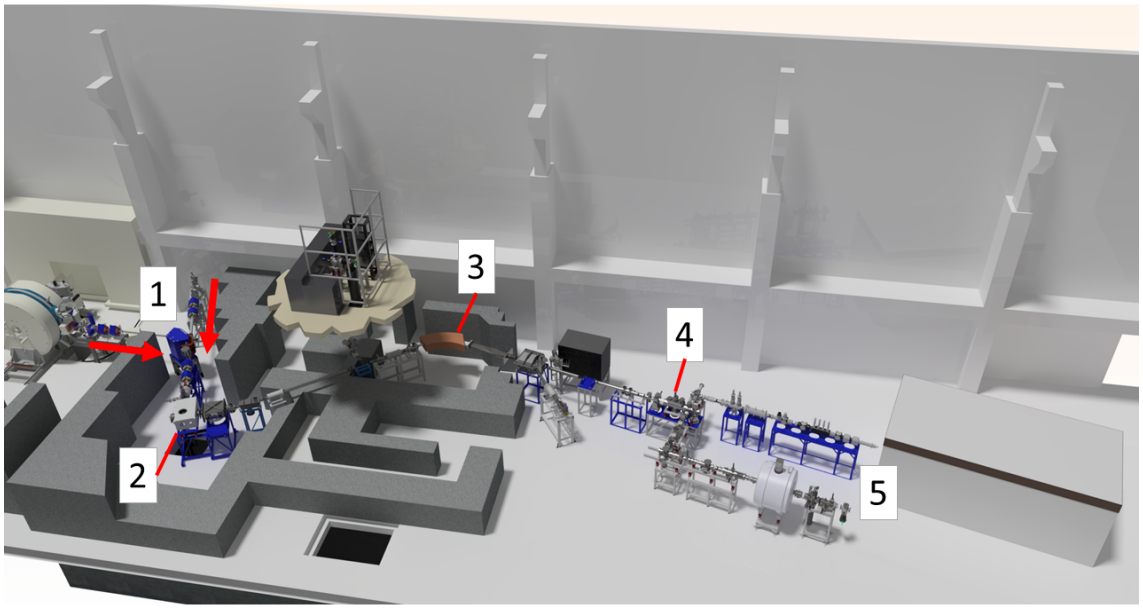

Figure 1. The layout of the IGISOL facility and beamline at University of Jyväskylä. 1. A high energy beam from a particle accelerator impacts the target at 2. The nuclei of a desired mass number are then separated from the resulting ion beam with the dipole magnet at 3. The buncher at 4. is used to cool and optionally bunch the separated beam before it is used in the measurement setups at 5.

ions having a large energy distribution, and thus a buncher is needed to improve the beam quality. To efficiently transport the ion beam in the facility, the behaviour of the beam needs to be understood.

3 Transport of ion beams

As ions experience the Lorentz force [16, 17]

$$\mathbf{F} = q \cdot (\mathbf{E} + \mathbf{v} \times \mathbf{B}), \tag{1}$$

where q and $\mathbf{v}$ are the charge and velocity of the ion, $\mathbf{E}$ and $\mathbf{B}$ are the electric and magnetic fields, ions can be controlled with electric and magnetic fields. From the ion source, the ions are transported to the measuring instrument using a beamline, where they travel in a long, continuous vacuum volume. A beamline consists of ion optical elements, which manipulate the ions by using electric and magnetic fields [18].

In beamlines transporting low energy (<100 keV) ions, devices based on electric fields are often preferred in ion transport, as the effect of static electric fields is independent of the mass of the ions. There is therefore less need to adjust the fields, as the focusing and steering effect on beams of same energy but different masses remains the same. In this work, only ion optical elements based on electric fields are considered. Such elements are comprised of one or more electrodes, which are essentially metal pieces attached to a tunable voltage supply.

Depending on the way the ion beam was formed, the beam in the system can be either continuous, bunched or have some time structure. As the name implies, a continuous beam is formed by ions entering the beamline without pauses, while a bunched beam is formed when a group of ions enter the beamline with regular intervals. Although the ion production method defines the initial time structure of the ion beam, a radiofrequency quadrupole cooler-buncher can be used to turn an ion beam with an arbitrary time structure into a bunched beam, as illustrated in figure 2.

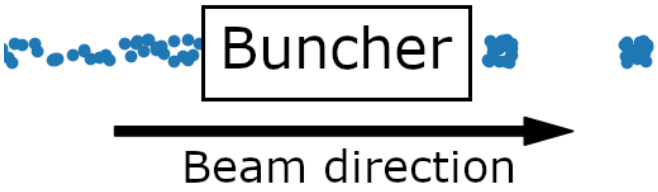

Figure 2. A buncher can be used to turn an ion beam of arbitrary time structure, such as a continuous beam, into a bunched beam.

3.1 Principles of ion optics

When dealing with ion beams in a beamline, the convention is to call the path along the middle of the beamline the optical axis and the plane perpendicular to it the transverse plane or the radial plane [19, 20], as seen in figure 3. For convenience, the direction the ions move on the optical axis is denoted the z axis, while the x and y axes lie on the transverse plane, perpendicular to each other and the z axis.

In an ideal case, all the ions would move in a line on the optical axis with zero spatial size and with the same kinetic energy. This is, naturally, unrealistic. Regardless of the ion production method, the ions always have some distribution of kinetic energies and directions, and positions on the transverse plane. As practically every ion has some transverse velocity, a beam flying freely expands in the transverse plane and eventually the ions will be lost as they will hit the walls of the beamline [17]. A beam of good quality thus moves as close to the optical axis as possible.

To accommodate the use of multiple ion sources and measuring instruments, a beamline is often split into multiple branches [1, 10, 13], although only one route from source to instrument is usually used at the same time. As most experiments benefit from having a large number of ions, an important property that can be defined for a beamline or any device within is its transmission [17], which is simply the percentage of ions that make it through the beamline or a device.

Due to the Lorentz force, ions are affected by changes in electric potential, which in beamlines is used to accelerate, decelerate, steer and focus the beam. The electric potential difference of the ion source and the beamline dictates the kinetic energy of the beam [13]. As the achievable beam energies using high voltage power supplies are quite low (<100 keV) [10, 13, 21] compared to what a particle accelerator give out [1, 13], these types of systems are known as Low Energy Beam Transport (LEBT) systems. Inside an ion beamline, if the ions can move freely, the trajectories and

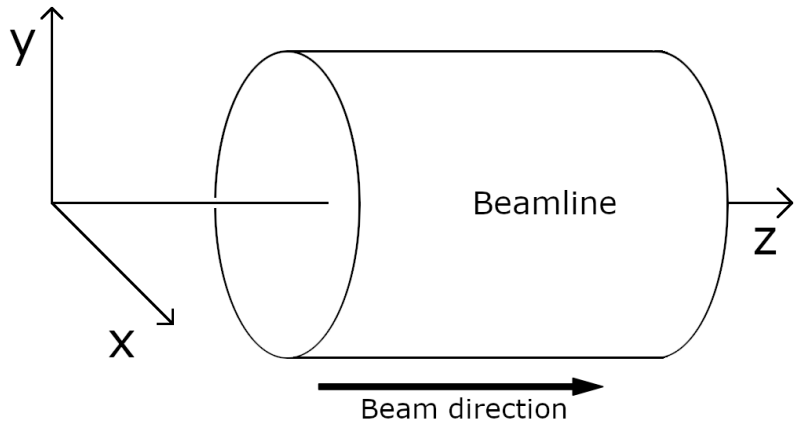

Figure 3. The coordinate system used in this work. The z axis is the optical axis of the beamline, while the x and y axes form the transverse plane.

behaviour of the ions is analogous to that of rays of light, in that the ions move in straight lines that can be bent using various ion optical elements, such as electrostatic lenses [18]. Such devices are used to improve the transmission of the beamline.

3.2 Electrostatic lenses

Electrostatic lenses are rather simple ion optical devices, that are used to keep the transmission efficiency of a beamline high by keeping the transverse size of the beam manageable. In its most basic form this is achieved by focusing the ion beam similarly to a converging lens in light optics. Such a lensing effect can be formed, for example, with a hollow metal cylinder or a thin metal plate electrode with a circular aperture [18]. The lens is placed so that the centre of the aperture lies on the optical axis to allow the beam to pass through and a potential is applied to the electrode. A dip or a bump is then caused in the electric potential near the lens. The further away from the axis an ion passes through the lens, the greater the change in its trajectory the potential gradient causes [18]. For ions moving parallel to the optical axis, the effect causes the ions to pass through a common focal point. The focal length of the lens depends on the energy of the beam, the geometry and the applied voltage, with higher energies increasing and higher voltages shortening the focal length [18]. Often the electric potential before and after the lens is the same, so the energy of the beam passing through a lens is not changed [22].

Another commonly used ion optical element is the electrostatic quadrupole. It consists of four hyperbolic rod electrodes arranged symmetrically around the optical

axis [23]. The electrodes opposite to each other are then set in the same potential so that the potential on the two pairs is not the same, which creates a quadrupole electric potential on the transverse plane. Unlike the simple aperture lens, an electrostatic quadrupole causes the beam to focus on one transverse plane and diverge on the perpendicular plane [23]. A quadrupole lens is thus commonly used to transform a beam asymmetric on the transverse plane, which can be caused by e.g. bending the beam through a corner in the beamline, into a round beam, which makes transporting the beam more efficient. By using multiple quadrupole segments, a total focusing effect can be achieved [23]. To quantify the behaviour of the ion beam and the effect of the various optical elements on it, a measure called emittance is used.

3.3 Emittance

Emittance describes the quality of the ion beam [17, 23]. It can be divided into transverse and longitudinal emittance. Transverse emittance is the phase space of the ions' position on the transverse plane and their transverse momentum, and as such it can used to determine whether the beam can physically fit in the beamline or through the various devices within. Longitudinal emittance, on the other hand, is the phase space of the energy and time of flight of the ions, which for a bunched beam can be thought to represent the length of a bunch. As the beam often needs to pass through narrow apertures and a bunch needs to be as temporally short as possible, a low emittance is desired [1, 11, 17, 23].

Emittance is commonly represented using geometric shapes, where the area of the shape gives the emittance value, and the shape itself and its orientation tell of the temporal behaviour of the beam [17, 23]. Both emittances evolve as the beam travels through the beamline, meaning that when considering the same beam at two different points in the beamline, the emittances would be different. It is possible to actively change the emittance of a beam using various elements found in the beamline, such as lenses, benders or bunchers, or by accelerating the beam, although the emittance also changes when the beam moves uninterrupted [17, 23]. When only conservative force fields ($\mathbf{E}$, $\mathbf{B}$) apply, only the shape and orientation of the emittance can be altered while the area (value) remains constant [23].

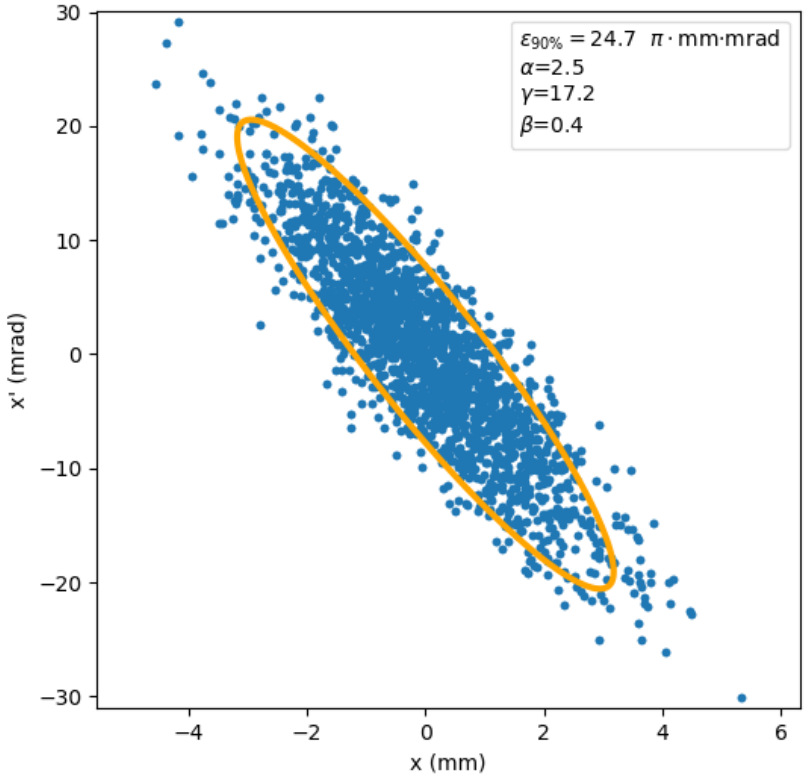

Figure 4. Emittance ellipse of 5000 simulated ions. 90% of the ions are inside the ellipse.

3.3.1 Transverse emittance

As the motion of the ions in a beam have two degrees of freedom perpendicular to the beam, transverse emittance can further be divided into x and y emittances that for freely moving ions are independent of each other [17]. For a symmetric beam the emittances in both directions are similar, while for an asymmetric beam they differ. With some devices, such as electrostatic quadrupoles, an asymmetric beam can be made symmetric. Nevertheless, the emittance in both directions evolve in the same manner and in this chapter, only emittance in the x direction is considered, and a similar treatment applies for the emittance in the y direction.

When dealing with transverse emittance, it is important to note that in different sources, the method for obtaining the value given for the emittance can differ somewhat, and as such one must be careful when comparing values. In this work,

the emittance is defined using the position x and dispersion x' of the ions. The dispersion is calculated from the angle formed by the transverse and longitudinal velocity, v_x and v_L respectively [17]

$$x' = \arctan(\frac{v_x}{v_L}). \tag{2}$$

As the x' depends on the tangent of the longitudinal and transverse velocity, it can be seen that when an ion is accelerated or decelerated, which increases the longitudinal velocity but ideally keeps the transverse velocity, the tangent decreases or increases respectively.

As the beam consists of ions each with their own position and velocity, it is possible to present each individual ion in a diagram where on the horizontal axis is the x position of the ion and x' on the vertical axis. Often the point cloud resembles an ellipse. The geometric emittance value is then given by the area of an ellipse drawn around the cloud [17, 23]. Usually the ellipse is drawn around 90 % of the points as some ions inevitably end up far away from the group and the emittance would lose its descriptive power if they were taken into account. It is important to note that other percentiles are also used. The area A of an ellipse is [23]

$$A = \pi R_1 R_2, \tag{3}$$

where R_1 and R_2 are the major and minor axes of the ellipse. As π is always present in the area of an ellipse, the geometric emittance is defined as [23]

$$\epsilon = R_1 R_2, \tag{4}$$

with units of [π·mm·mrad], although again to note, in some sources the emittance is given in units of [mm·mrad].

Since acceleration changes the longitudinal velocity and thus the value of x' of an ion, it causes the ellipse to vertically either decrease or increase in size. As such, acceleration does not preserve the area of the ellipse, and so the value of emittance of a beam before and after acceleration can't be directly compared. In the case of non relativistic velocities, the initial and the final (accelerated) emittance are related by [17]

$$\epsilon_2 = \epsilon_1 \sqrt{\frac{E_1}{E_2}}, \tag{5}$$

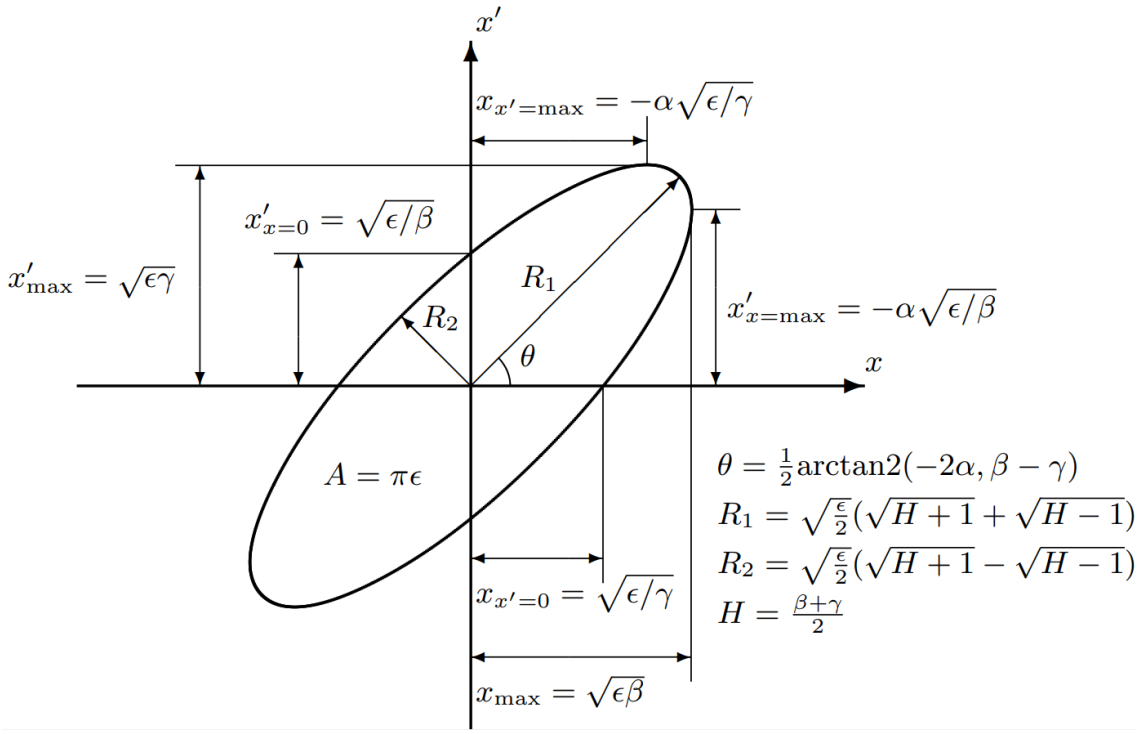

Figure 5. The shape and size of the emittance ellipse can be defined using the emittance ϵ and the Twiss parameters α, β and γ. Figure from [23].

where ϵ_1 and E_1 are the initial, and ϵ_2 and E_2 the final emittance and longitudinal energy. Thus, the energy of the beam needs to be give along with the emittance to make comparing the values, and thus beam quality, possible.

To determine the emittance of a beam, an ellipse can be fitted around the (x,x') point cloud. The equation for an ellipse centred on the origin is [23]

$$\gamma x^2 + 2\alpha x x' + \beta x'^2 = e, \tag{6}$$

provided that

$$\gamma\beta - \alpha^2 > 0, \tag{7}$$

where γ, α, and β are known as the Twiss parameters that determine the aspect ratio and orientation, and ϵ determines the area of the ellipse. Fitting an ellipse around some percentage of points is difficult, as there are infinitely many possible shapes. A statistical method of calculating the so called rms-emittance [23] is thus often employed, although it is not used in this work. An example of emittance ellipse fitting can be seen in figure 4.

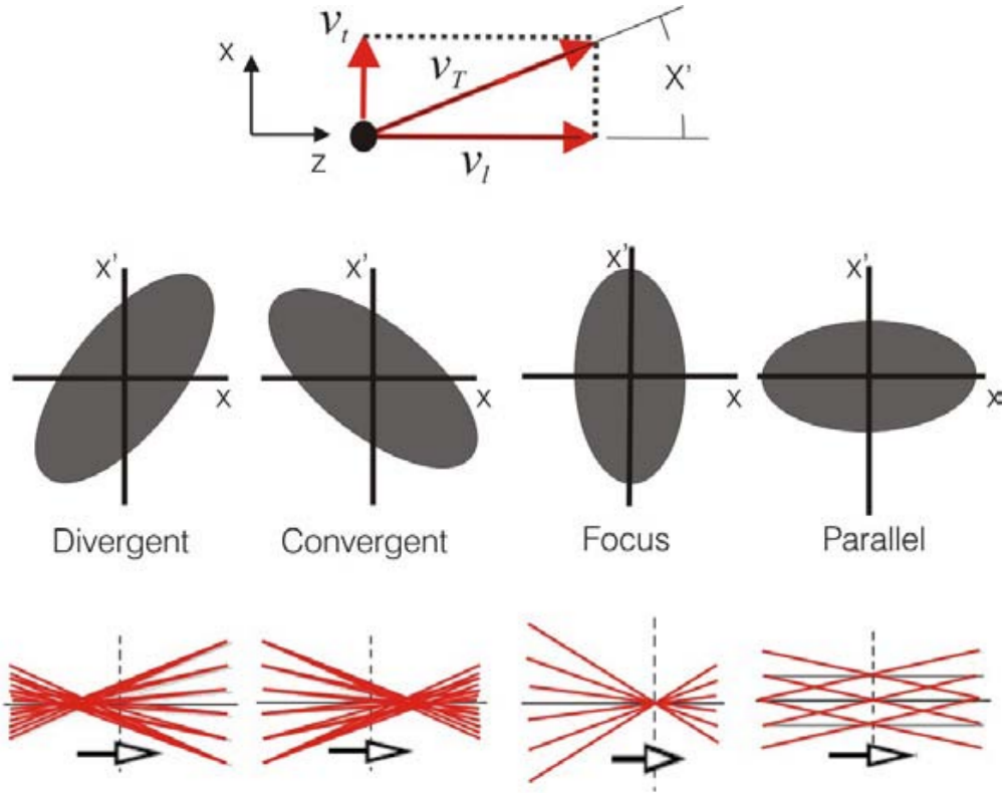

Figure 6. The different possible orientations of a transverse emittance ellipse. V_t, V_T and V_l are the transverse, total and longitudinal velocities respectively, while x is the position coordinate perpendicular to the beam direction z, and x' the angle between the total and longitudinal velocity of an ion. Figure from [17].

As the emittance is defined using the position and velocity of the ions, it is obvious that it evolves over time when observing the emittance of an ensemble of ions at consecutive points in the beamline. For this reason, the orientation and shape of the emittance ellipse changes when considering the emittance at consecutive points, although the area of the ellipse stays constant, if the force acting on the beam is conservative [23]. If the emittance is said to change, which requires non-conservative forces to act on the ions, it means that the area of the ellipse changes.

The emittance diagram has four regions, within which the ions have similar characteristics. The ions in the upper half of the diagram have positive velocity in the x direction, while the ions in the lower half have a negative velocity, and the ions on the right half of the diagram have positive x position, while the left half contains ions with negative x position. As such, ions in the top right quadrant are on the positive side of the x axis and are moving even further, in the bottom right the ions have a positive x position, but are moving towards the centre and

into the negative x values. On the bottom left the ions have a negative x position and they keep moving further into the negatives, while on the top left the ions have negative x position, but are moving towards and beyond the centre. If the ions experience no force, the velocity stays constant, and so each individual dot in the diagram moves only horizontally. It can then be seen that the major axis of the ellipse eventually always turns to lie in the top right and bottom left quadrants, when considering the emittance of the beam at consequent points in a beamline. The result is quite intuitive, as with nothing stopping the ions with transverse velocity, they keep moving further away from the axis. As any beam ultimately has a tendency to diverge, the beamline cannot consist only of drift space and measuring instruments, but various focusing elements, such as electrostatic lenses, must also be present.

The orientation of the ellipse makes it possible to determine whether the beam is converging or diverging [17, 23], the possible orientations are shown in figure 6. Following the previous explanation, it is clear that a beam in a top right-bottom left orientation is diverging, while in a top left-bottom right orientation the beam is converging. In between, a beam with vertical emittance ellipse is at its focus, meaning that the physical width of the beam is the smallest, but not zero. These results can be deduced by remembering that on the horizontal axis of the diagram is the ion's distance from the centre of the beam, and the vertical axis tells whether the ion is moving towards or away from the beam centre.

While the emittance is a property of the beam that describes the quality of the beam, a closely related property is the acceptance of any device or optical element used in the beamline. Acceptance defines the shape and size of the emittance of a beam that can pass through the device uninterrupted, with any ions outside the acceptance being lost [17, 23]. On the diagram, the horizontal axis shows how far away from the axis the ions can be before colliding with the device, while the vertical axis shows from how wide angle the ions can come. As there are usually multiple devices in a beamline, the acceptance of the beamline can be determined from the individual acceptances of the devices. To check if the beam can go through a device, the emittance of the beam and the acceptance of the device can be placed on the same diagram, and any ion outside the acceptance region collides either with the obstacle or with the beamline walls shortly after the device [17, 23].

3.3.2 Longitudinal emittance

Longitudinal emittance describes the quality of the beam in the direction of the beam. For bunched beams, longitudinal emittance governs how close the bunch is to its temporal focus and whether the bunch is elongating or contracting [17, 23]. Since each ion has slightly different kinetic energy and occupy different positions longitudinally, they arrive at any given observation plane at different times. The ions' longitudinal kinetic energy E_l at the plane and time of flight t from some given moment to the plane can then be presented in a (E_l,t) diagram. The value for longitudinal emittance is then the area of the shape drawn around the scatter plot, which for longitudinal emittance is also often elliptical. The emittance can also be calculated statistically from [17]

$$\epsilon_{long} = E_{FWHM} \cdot t_{FWHM}, \tag{8}$$

using the widths of the energy and time-of-flight (also known as temporal) distributions. As in the case of the transverse emittance, the shape of the plot can be used to determine features of the bunch.

The bunch is said to be (longitudinally) in time focus when the axial positions of the ions in the bunch are as close to each other as possible. As the ions with higher energy i.e. greater velocity eventually pass slower ions, the width of the time-of-flight distribution of the bunch first shrinks until the time-focus plane is reached, after which the distribution grows.

As the kinetic energy of each ion stays constant, but the ions with less energy lag behind, over time the ellipse turns clockwise. The major axis of the longitudinal emittance ellipse eventually turns to lie in the top left-bottom right quadrants. It is then clear that an ellipse in a top right-bottom left orientation is still shortening, a vertical orientation indicates that the bunch is at its focus, and a top left-bottom right orientation means that the bunch is past its focus and is elongating.

As the energy spread of an ion bunch is hard to measure, longitudinal emittance is not often used in actual measurements. Instead, a more important measure of the quality of a bunched beam is the temporal bunch width.

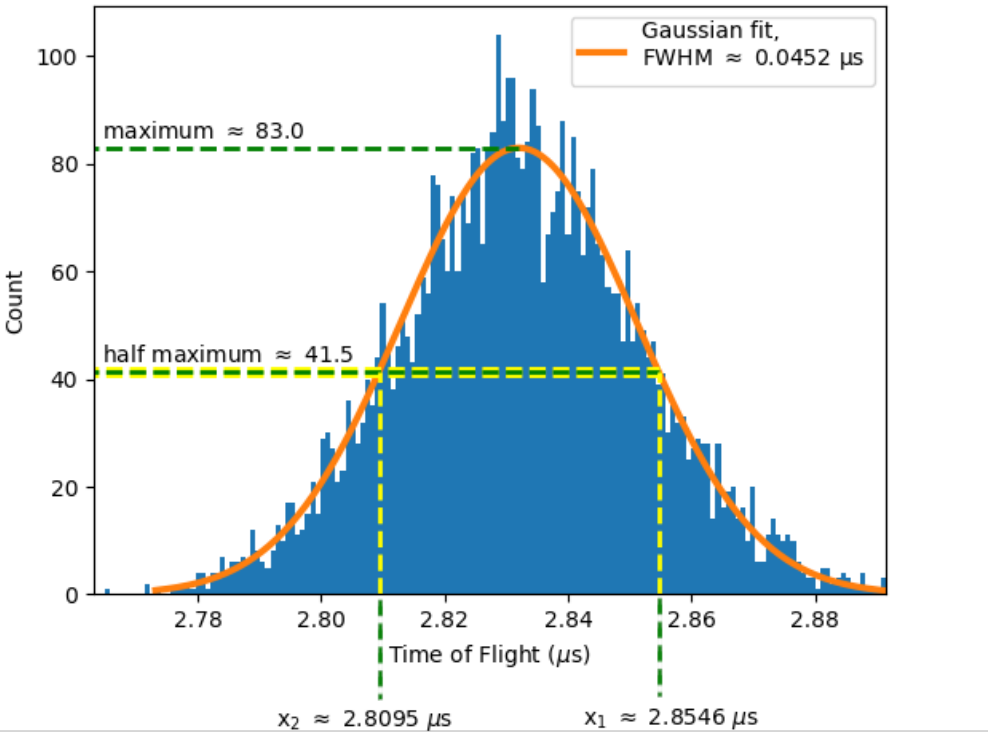

Figure 7. Time of flight distribution of an ion bunch and the data points required for graphically determining the full width at half maximum.

3.4 Temporal width of an ion bunch

An ideal ion bunch would be a zero-width cloud of ions each with the same energy, but in reality the ions again have a distribution of positions and velocities. The (longitudinal) length and energy spread of a bunch are determined from the time-of-flight (ToF) and energy distributions of the ions respectively. In practice, a single-ion sensitive detector, such as a microchannel plate detector (MCP) can be used to measure the ToF distribution [17, 24], while measuring the energy distribution is more difficult and is commonly considered only in simulations. The distributions are formed by recording the time at which each ion crosses the transverse plane of interest and the energy of the ions at the plane.

The ToF and energy spread of a bunch is often indicated using full width at half maximum (FWHM), also called just the width, of the respective distributions. Often both distributions are close to Gaussian, from which the FWHM is calculated [8, 25,

26]. The width of a Gaussian distribution can be calculated using [27]

$$\text{FWHM} \approx 2\sqrt{2\ln 2}\sigma, \tag{9}$$

where σ is the standard deviation

$$\sigma = \sqrt{\frac{1}{\text{N}}\sum_{i=1}^{N}(x_i - \mu)^2}, \tag{10}$$

where N is the number of ions, x_i the ToF or energy of each ion, and μ is the mean of the distribution. As the length of a bunch changes over time, the point at which the temporal width of an ion bunch is at its smallest is called the time-focus plane.

In addition to calculating the width, it is also possible to determine the width by plotting a histogram of the values and fitting a Gaussian curve on the plot. The width is then the difference of the independent values where the curve reaches half of the maximum value. To get reliable results, the bins of the histogram must be of appropriate width, i.e. a single bin shouldn't contain every occurrence but neither should the bins be so narrow that most of them contain no counts. A large number of data points is thus required to obtain a proper fit, and for few occurrences, the equation (9) is used. The widths obtained by calculation and fitting can differ somewhat, depending on the quality of the fit and as the calculated width can be more sensitive to extreme values for small number of data points. An example of a Gaussian fit on a time of flight distribution is shown in figure 7. The widths presented in this work are from fitted curves.

In some cases, the distributions can become skewed. A beam moving through a volume where gas is present, is one common example: some ions flying through gas can collide with the particles and lose energy, leading to a longer time of flight. A skewed distribution can result in reduced transmission efficiency, as more ions are outside the determined width than expected. The likelihood of ion-gas collisions can be estimated using the mean free path of the ions.

3.5 Mean free path of an ion

To efficiently transport the ion beam, there has to be a good vacuum inside the beamline. A collision between an ion and a gas particle can cause the ion to lose kinetic energy or give it transverse momentum, likely leading to lower transmission. For a given volume and temperature, the density of gas particles, and thus the collision frequency, is determined by its pressure [16]. In order to reduce the amount of collisions, a beamline is typically pumped into a high vacuum ($\sim 10^{-6}$ mbar) [10, 17]. The desired degree of vacuum required can be determined by examining the length of the mean free path, i.e. the average distance between two collisions.

The length of the mean free path is dependent on the pressure and temperature of the gas, and velocity of the ion, in addition to the cross section area of the gas particles and the ion [17, 28]. A more thorough analysis on calculating the mean free path is done in chapter 4.3.2, but as an example, an ion of mass 100 u with 5 keV of kinetic energy moving through 10^{-6} mbar helium at 20 °C has a mean free path of tens to hundreds of metres. In LEBT beamlines, the distance from the ion source to the measuring instrument is typically in the range of some tens of metres [11]. It is thus unlikely that an ion would collide with a gas particle at that pressure, although since a beam consists of a huge amount of ions, collisions are bound to happen. Keeping the beamline at a high vacuum is deemed to be the sweet spot between practicality and efficiency.

Although a good vacuum during beam transport is desired, in some devices gas is introduced into it to purposefully slow down the ions. At pressures of 10^{-2} mbar in helium, the mean free path drops to millimetre range. In a buncher, this is taken advantage of as the gas is used to cool the ions due to the frequent collisions reducing the energy spread of the ions [8, 17, 23].

Since the beam travels in various degrees of vacuum and the beam consists of individual ions, the Coulomb interaction between ions can push the ions away from each other. The so called space charge effect can increase in the transverse size of the beam.

3.6 Space charge

As charged particles, each ion experiences the Coulomb force caused by other ions [16]

$$\mathbf{F} = \frac{1}{4\pi\epsilon_0}\frac{q_1 q_2}{r^2}\hat{\boldsymbol{r}}, \tag{11}$$

where ϵ_0 is the vacuum permittivity, q_i the charges of the ions, and r their mutual distance. Since the beam consists of ions of the same polarity, i.e. the ions repel each other, the resulting space charge effect causes the beam to diverge and in practice also increases the emittance as a function of time [17, 23]. A major component affecting the strength of the effect is the charge density of the beam. The effect of charge density is intuitive, as more ions closer together repel each other stronger.

When considering a beam with a uniform charge distribution, meaning that the distance between nearest ions is constant throughout the beam, the space charge effect doesn't affect the emittance of the beam and the effect of the space charge on the beam is easily calculated [23]. Unfortunately, the charge distribution is rarely uniform, but instead often resembles a bi-Gaussian distribution, where more ions are packed close to the optical axis while less ions are found near the edge of the beam. In this case, the emittance of the beam increases over time, and the exact effect on the beam must be estimated numerically [23]. Various models have been devised to approximate the effect, as a beam contains too many ions to calculate all the interactions [17, 23].

The ion beam currents in LEBT systems, however, are typically low enough that the effect on the beam is negligible. In such systems, the space charge effect can become an issue in ion traps such as bunchers, where a cloud of ions mutually interacts for a long period of time and can cause ions to be lost. The beam currents in this work are assumed to be so low that the space charge effect is mostly ignored, with only one set of simulations considering the effect.

4 Radiofrequency quadrupole cooler-buncher

The radiofrequency quadrupole (RFQ) cooler and buncher is a device that accepts an ion beam with arbitrary time structure and gives out a cooled and optionally bunched beam. Often bunches with short temporal spread and small energy distributions are desired [8, 10]. The ions entering the device are trapped and their motion is manipulated with the use of static and time-dependent electric fields [19]. In the device, a low pressure buffer gas is used to cool the ions [17], which refers to reduction in the amplitude of the ions' axial and radial motion.

In this chapter, first the structure and operation of a simple buncher is explained, followed by an explanation on the operation and considerations of an actual buncher in a beamline. Lastly, as the buffer gas plays an essential role in the function of the device, two possible options for modelling the ion-gas interactions in simulations are presented, with an explanation on why the hard sphere collision model was used in this work.

4.1 A simple RFQ cooler-buncher

A very simple buncher consists of four long parallel round rod electrodes arranged symmetrically around the optical axis, with a thin plate electrode at both ends of the rods [19, 20], illustrated in figure 8. Ions are injected into the buncher through a small aperture in one plate electrode, and typically extracted through the other plate, likewise with an aperture. The ions are trapped inside the buncher by creating a radial and an axial minima in the electric potential. The radial minimum is formed by applying alternating voltage to the rods, so that the rods opposite to each other are in phase, while the adjacent rods are in the opposite phase [19, 20]. The axial minimum is formed on the optical axis by applying a static voltage on the end plates.

The time-dependent electric field formed by the rods creates a rotating saddle potential on the transverse plane, as illustrated in figure 9. Over a period of the signal an ion in the potential experiences a total force either pushing it towards the axis, leading to radial confinement, or away from it. Whether an ion is confined or

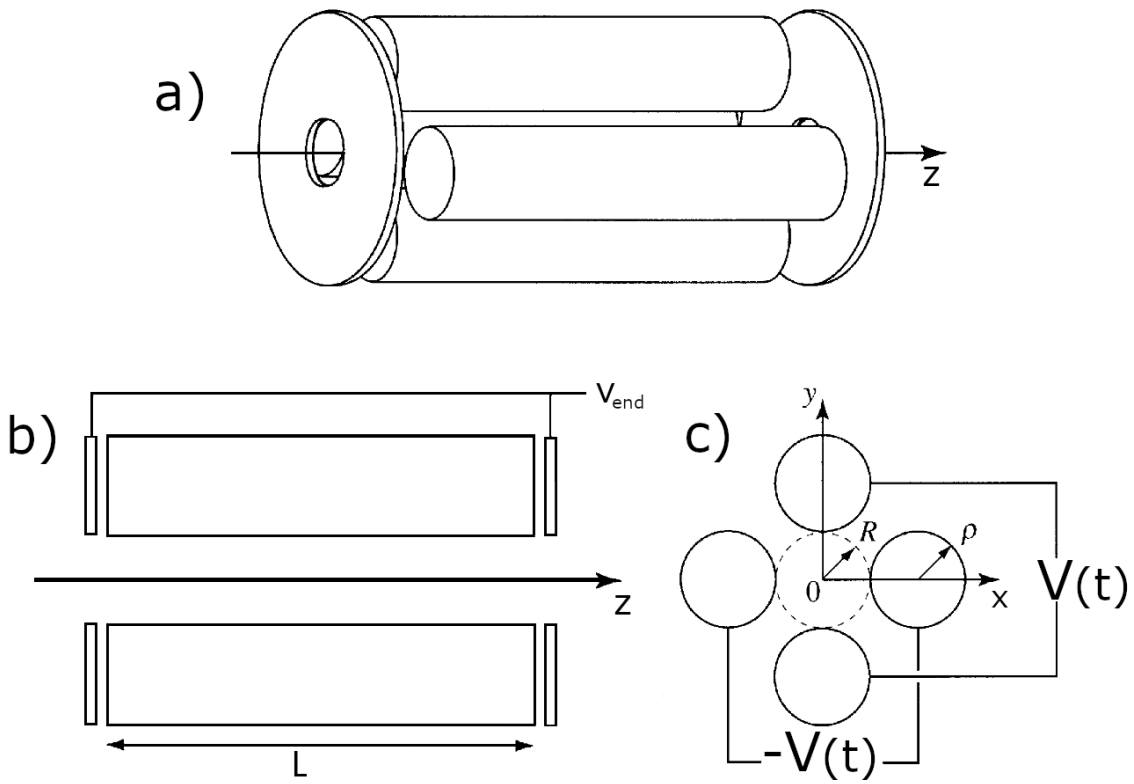

Figure 8. a) A simple buncher consists of four RF rods and two end plates. The ions move along the optical axis. b) Side view of the device. Voltage V_{end} is applied to the end plates to stop ions from escaping. c) Cross section of the buncher. An alternating voltage is applied to the rods, with the voltage on neighbouring rods in the opposite phases, which confines the ions radially. The ratio of the rod radius ρ and their distance from the axis R affects the performance of the trap. Figure from [20], modified.

not depends on the mass and charge of the ion, and the amplitude and frequency of the voltage. In order to confine ions of various masses, the amplitude and frequency of the alternating voltage applied to the rods needs to be adjustable.

In order to cool the confined ions, a buffer gas is present in the buncher. The trapped ions collide with the gas particles, reducing their energy [17]. As the ions cool down and lose their radial velocity, they end up oscillating closer to the axis of the trap, i.e. their motional amplitude shrinks. The same happens axially, resulting in ions cooling to the axial potential minimum. After sufficient cooling time, the ion bunch collected in the axial minimum is released by lowering the potential on one of the end plates. The motion of an ion in a buncher can be expressed with the so-called Mathieu equations, which can be used to determine if the motion of an ion of particular mass and charge is stable [19, 20].

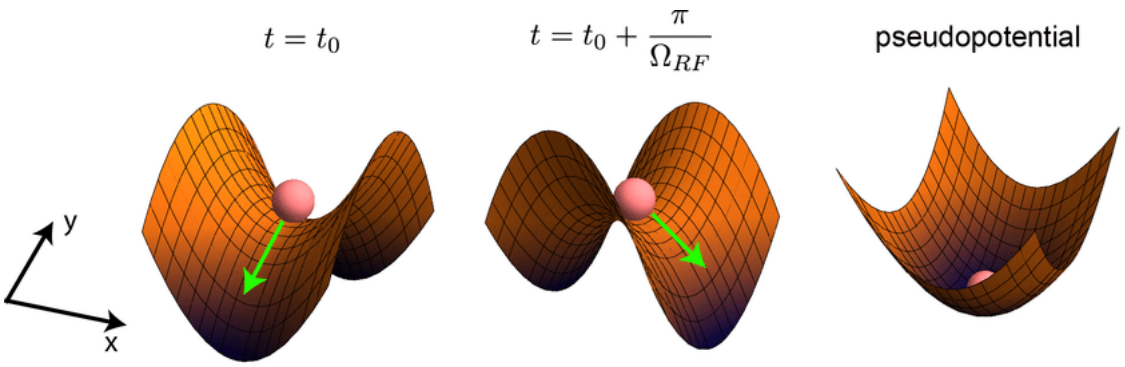

Figure 9. The alternating voltage applied to the four rods creates a rotating saddle potential. If the amplitude and frequency of the voltage are appropriate to the charge and mass of the ions, over one period the ions experience a time-average parabolic potential with a minimum on the axis confining the ions radially. Figure from [20].

4.1.1 Ion motion inside of an RFQ

To get a sense of what is required for radial confinement, the equations of motion for an ion in a buncher with no buffer gas can be analysed. In an ideal case the electric potential created by the rods would be quadrupole, but due to the design of the device, higher order harmonics in the potential are present [17, 19]. A major cause of the harmonics is the use of round rods instead of hyperbolic, but round rods are often used as they are easier to manufacture [17, 29]. It has been found that the strongest harmonic perturbations can be minimised by choosing the radius of the rods ρ and the distance from the axis to the surface of the rods R to be around [29]

$$\frac{\rho}{R} = 1.1465. \tag{12}$$

In the case of a pure quadrupole field, away from the end plate electrodes the electric potential ϕ takes the form [19]

$$\phi(x,y,t) = \frac{x^2 - y^2}{2R^2}(U_0 + V_0 \cos \Omega t), \tag{13}$$

where x and y are the transverse directions, U_0 the potential at the end plates, V_0 the peak amplitude of the voltage on the rods, Ω is the angular frequency of the voltage, and R is the distance from the axis to the rods. As the potential in a buncher is not exactly quadrupolar, this doesn't quite apply, but close to the axis of the device

this is a good approximation of the potential [19]. In this potential the equations of motion, known as the Mathieu equations, for an ion are

$$\ddot{x} = -\frac{q}{mR^2}(U_0 + V_0 \cos \Omega t)x, \quad \ddot{y} = \frac{q}{mR^2}(U_0 + V_0 \cos \Omega t)y. \tag{14}$$

The stability of the radial motion can be expressed with the help of the so-called Mathieu parameters a_i and q_i that can be substituted in the equations (14)

$$a_x = -a_y = \frac{4qU_0}{m\Omega^2 R^2}, \quad q_x = -q_y = \frac{2qV_0}{m\Omega^2 R^2}, \quad \tau = \frac{\Omega t}{2} \tag{15}$$

It can be shown that the ion's radial motion is stable only in certain regions of the (q_i,a_i) space [19], which can be shown in what is known as a stability diagram. Using the relation between the parameters in x and y directions, the stable regions of both directions can be placed in a single diagram, shown in figure 10. From this diagram, it can be seen that the motion in both directions is stable only in select few regions. The diagram can then be used to select the voltages and frequency of the rods in the trap that radially confine an ion of a given mass and charge. In practice, only the stable region near the origin is used in ion trapping [3, 10, 17, 19], as the regions further away would require extreme values for some of the values in the Mathieu parameters. Since the frequency of the alternating voltage used in a buncher is usually in the range of hundreds of kHz, the rod electrodes are commonly known as radiofrequency (RF) rods.

As the radial confinement is the result of the rods pushing and pulling the ion, the alternating voltage causes the ion to oscillate around the optical axis [17, 19]. This motion can be divided into macro and micro motions. An analogy for these motions would be two sinusoidal signals of different frequencies and amplitudes added together. Similarly, the motion of an ion is a combination of two circular motions. Even though the ions can be confined with a range of Mathieu parameters, i.e. voltages and frequencies, the amplitude and frequency of the induced motion depends on the chosen values.

An ion's axial motion is less complicated, as the time-dependent fields cause only radial forces. In axial direction, the ions are controlled by simple potential gradients formed with electrodes using static voltages [17, 19]. As long as the potential barriers formed by the plate electrodes at the ends of the buncher are higher than the kinetic energy of an ion, it stays axially confined.

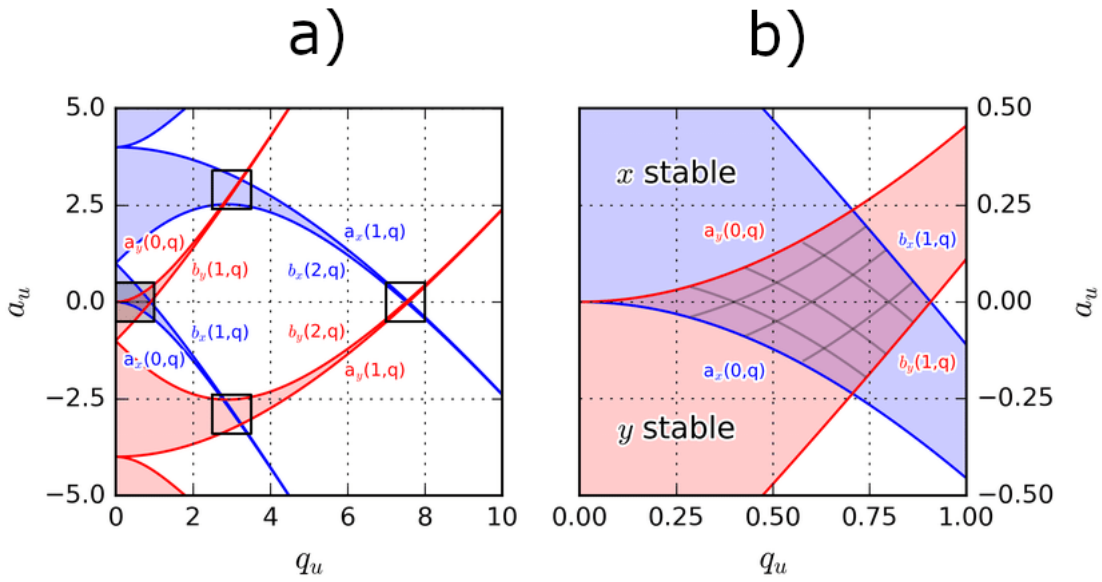

Figure 10. a) The stability diagram of a buncher. Stability in both transverse directions is shown in a single diagram, indicated by the red and blue regions. The value of parameters a_u and q_u are determined by the mass and charge of the ion, and the frequency and amplitude of RF voltage, and the depth of the axial potential. To keep the ions confined, the motion in both directions must be stable, indicated by the overlapping regions. b) Only the stable region near the origin is commonly used. Figure from [30].

Since the random collisions between an ion and the buffer gas can increase or decrease the energy and change the direction of the ion, the Mathieu equations don't apply exactly as presented [17, 19]. By using a simple drag model for the gas the effect can be analytically examined, but usually computer simulations utilising more complex gas models are used [17, 19]. Similarly, the space charge effect can alter the stable regions of the parameters, as the Mathieu equations only consider a single ion in the trap. Nevertheless, the presented equations form a solid understanding on the stability of an ion's motion in a buncher.

Although understanding the motion of the ions in a buncher is important, in order to design a buncher that performs well in a beamline, more than the stability of the ions must be considered. Just as important is the ability to efficiently get the beam into and out of the buncher.

4.2 Realistic buncher

When considering an actual buncher in a research facility, the device has to work with good efficiency. Namely, a poor quality beam needs to be efficiently transferred into the device, and a good quality beam needs to be transferred out. A good bunched beam is characterised by short temporal spread and small energy distribution, low transverse emittance, and a properly adjusted time-focus plane. A buncher should also have high overall transmission efficiency. A typical buncher consists of four main sections: injection optics, main RFQ section, one or more bunching sections, and extraction optics [10, 25].

First, the beam to be cooled and bunched enters the device with the help of injection optics, which consists of an arrangement of electrostatic aperture lenses used to focus the beam into the main RFQ section through a small aperture. In the main section and the bunching sections, the ions are confined with the use of static and RF electric fields and cooled via collisions with a buffer gas. A potential gradient in the main section is used to transfer the cooled ions to the bunching section designed to have finer control on the potential, as the shape of the axial potential before and during extraction affects the quality of the bunches. The cooled ions are then extracted from the bunching section as ion bunches and are then focused to fit into the beamline using extraction optics consisting of an arrangement of electrostatic lenses.

In this work, a complete buncher comprised of the injection optics, main RFQ section, two bunching sections, and extraction optics was designed. As the parameters of the incoming beam were known, the device could be tailored to provide the type of bunches required at FAIR using the available beam. Next, a more in-depth description of the different sections in a typical buncher are given, followed by a look into the factors determining the quality of the bunches.

4.2.1 Main RFQ section

The main RFQ section is conceptually the same as the simple RFQ described above in section 4.1. Here, the injected ions are stopped and cooled by a low pressure buffer gas, while a rotating quadrupole electric potential created by four parallel rods confines the ions radially. The main section is typically quite long, as fast moving and heavy ions require more distance to be stopped. To transfer the ions to the bunching section, there needs to be a potential gradient that allows the ions to flow "downhill" from the entrance. In many existing devices, this is realised by dividing the RF rods into short segments that share the RF components but the DC components are isolated from each other [10, 25]. This way an axial potential gradient can be created by applying lower voltage to each consecutive ring of segments, starting from the injection side. A ring of segments refers to a set of four segments that lie on the same transverse plane. As a sum of the DC and RF voltages, the ions experience a force that keeps them on the axis, but transfers them to the axial minimum in the bunching section [19, 26].

However, creating the gradient with segments doesn't come without issues. Using long segments creates flat regions in the axial potential, resulting in a gradient that more resembles a descending staircase than a steady downhill. This can lead to ions even stopping in the constant potential part and thus it can take unreasonably long for the ions to get through the buncher. Then again, if very short segments are used, there has to be more of them, complicating the RF and DC voltage distribution to the electrodes bringing up the cost of the device and increasing the need for maintenance. Nowadays other methods of creating the gradient are experimented with [25].

In this work, the gradient is formed not by dividing the rods, but by placing two geometrically identical wedges shaped like right triangles next to each other with the shorter base facing the opposite way between each of the adjacent rods, for a total of eight wedges, as shown in figure 11. Then a higher potential can be applied to the wedges whose bases face the injection side, and lower potential to the wedges with bases closer to the bunching section. Near injection, more surface area of the wedges in higher potential is exposed to the volume, while near extraction, more surface of the wedges in lower potential is exposed. On the axis, a smooth electric potential gradient, where the potential is higher on the injection side and lower on the extraction, is thus created. By using this method the whole system becomes

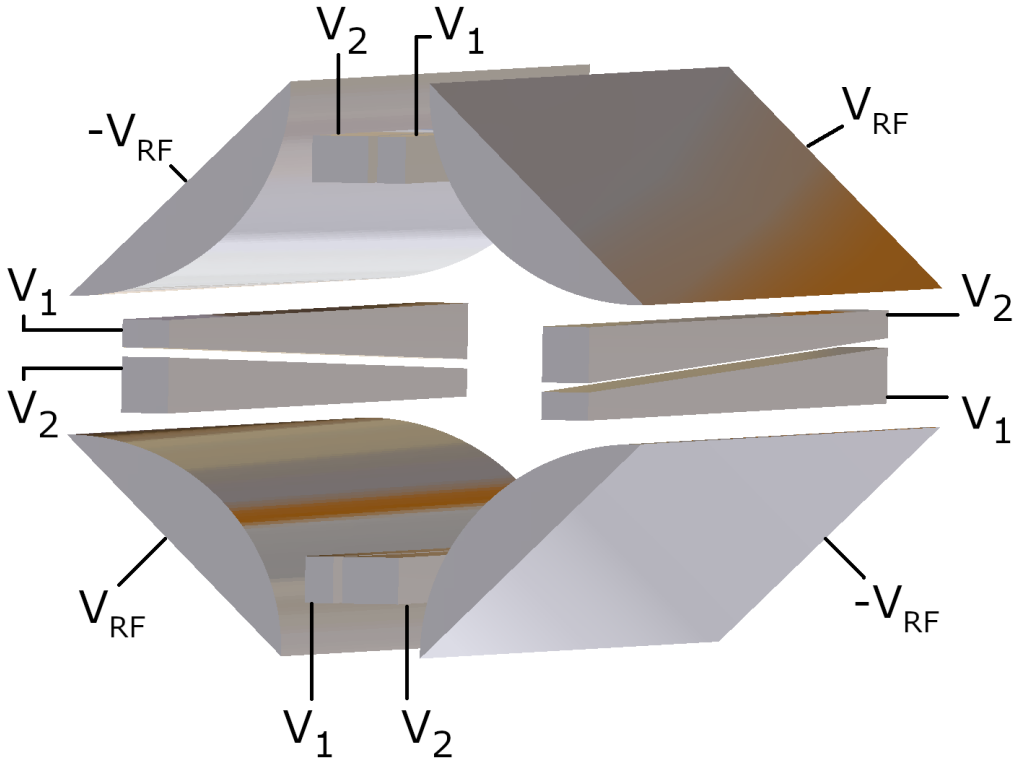

Figure 11. The arrangement of RF rods and wedges in the buncher, with other parts not visible. The wedges are arranged so that near injection, more surface area of the wedges in higher potential V_2 is exposed to the volume than the wedges in lower potential V_1, while near the bunching section it's the opposite. This creates a smooth potential gradient transferring the injected ions to the bunching section. The neighbouring RF rods are in the opposite phase of the RF signal. The perspective makes the device look deceivingly short, as the RF rods are much longer than the distance between them. Exact dimensions can be found in chapter 6.1.1.

much simpler, as the gradient transferring the ions to the bunching section can be created with only eight electrodes.

4.2.2 Bunching section

The structure of the bunching section is otherwise quite similar to the main RFQ, but it is often considerably shorter, only some centimetres, as the ions entering the section are already cooled in the main section. Before extraction the ions are collected in an axial minimum created in the bunching section, from which the collected ions are then extracted as ion bunches. Instead of DC wedges, the bunching section contains multiple few millimetres long RF segments, as this allows for better control of the

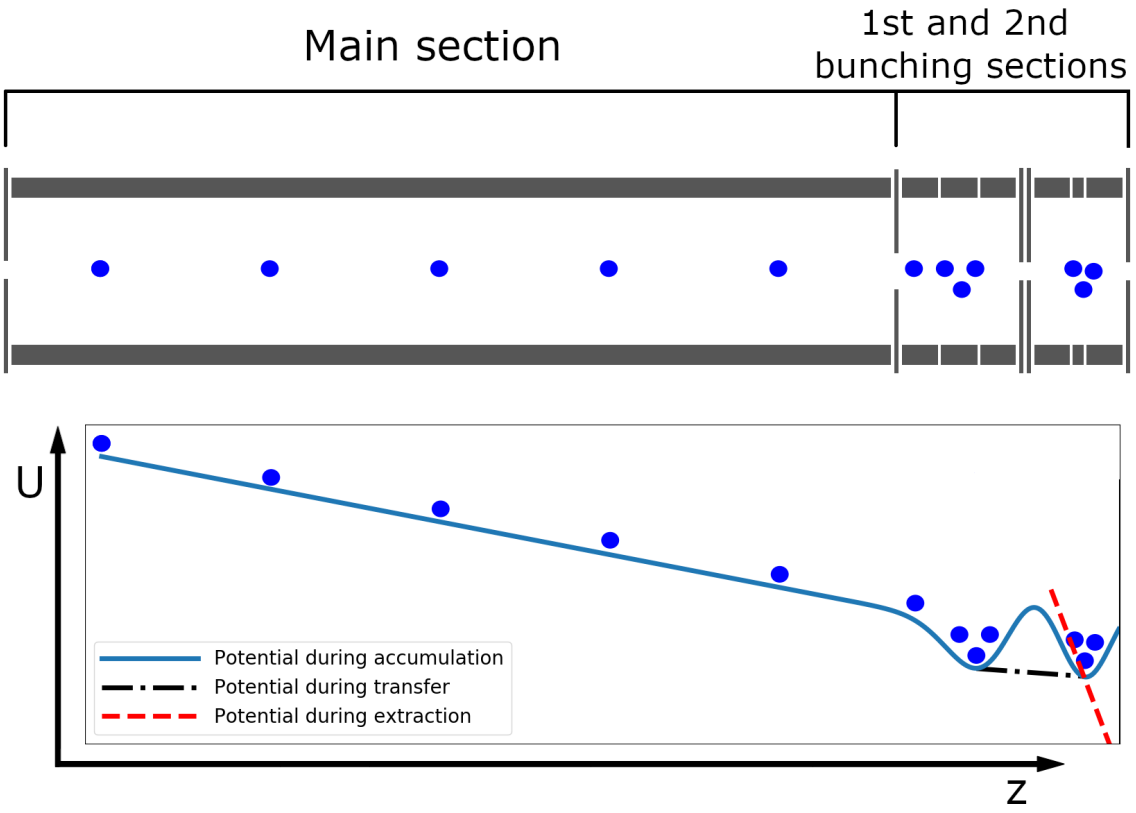

Figure 12. Illustration of the buncher and the electric potential during accumulation, transfer and extraction phases. A descending potential transfers the injected ions through the main RFQ section to the first bunching section, where the ions are accumulated. From the first bunching section the ions are then transferred to the second section with a lower pressure by lowering the voltage in the plates between the sections. After some final cooling in the second section the ion bunch is extracted from the buncher by switching the voltages on the plates.

axial potential. The DC component of each ring of segments can be set separately to precisely adjust the potential on the axis.

The bunching section is separated from the main section by a barrier, such as a plate with an aperture on the axis. If the buffer gas is fed into the main section, the plate significantly restricts gas from flowing into the bunching section keeping the pressure low, while still allowing the cooled ions on the axis to pass. Together with another plate with an aperture placed at the end of the section, the ions are confined axially.

Although the gas plays an essential role in the operation of the buncher, controlling the pressure in the bunching section is important, although also challenging. Gas is

needed in the main section to cool the incoming ions and some gas is needed in the bunching section to cool the ions flowing in from the main section. On the other hand, too much gas in the bunching section increases the amount of ion-gas collisions during extraction. This increases the energy spread of the extracted bunch and thus can widen the ToF distribution and lead to a reduced transmission efficiency [8, 17].

To extract the cooled bunch, the potential on the plate behind the bunch is switched to a higher value and on the plate in front is lowered, which creates a downward gradient in the potential allowing the ions to fly out. The steepness of the gradient together with the extraction optics define the time-focus plane of the buncher [31]. In typical operation, the time between operation cycles, i.e. bunch releases, is in the range of milliseconds [3, 25], depending on the desired level of cooling.

In this work, the designed buncher contains two bunching sections. This allows for accumulating one bunch of ions, while another is being extracted. This requires three phases in the operation: accumulation, transfer and extraction. First, the ions are allowed to accumulate in the first bunching section. The cooled bunch is then moved to the second bunching section, where the ions are allowed to cool for a moment before extraction. Figure 12 shows the potential inside the buncher during these phases.

As the transfer to the second bunching section induces some undesired motion, the pressure in the section must be chosen so that it allows for some cooling, but doesn't affect the quality of the extracted bunches too much. If the gas is fed into the main section, the pressure in the bunching sections is defined mainly by the pressure in the main section and the plates separating the sections, as they prevent the gas from flowing freely. To efficiently get the ions into the main section and out of the bunching section, injection and extraction optics consisting of a set of electrostatic lenses are used, respectively.

4.2.3 Injecting and extracting a beam

As the ions in a LEBT beamline typically have energies in the order of keVs [8, 20], the ions entering the buncher need to be slowed down to an injection energy of tens to a couple hundred eVs, as higher energies would require unreasonably large volume to stop them. In addition, the beam in the beamline is often wider than the aperture leading into the buncher, requiring focusing to keep a high transmission. Similarly, the extracted beam needs to be accelerated and focused to reach the subsequent instruments.

To decelerate the beam, the buncher is set on a high voltage platform, meaning that all the parts of the buncher have a higher electric potential than the beamline before or after the device. The difference between the kinetic energy of the beam and the potential inside the buncher determines the injection energy and so the energy of the beam needs to be slightly higher than the potential. The energy of the beam after extraction is also defined by the difference between the potential in the bunching section and the following beamline with some additional energy imparted by the extraction process.

To inject the beam of ions into the buncher, a set of electrostatic lenses, known together as the injection optics, is used. Similarly, a set of lenses make up the extraction optics used to focus the extracted beam. Often the lenses have differently sized apertures, with the lens closest to the buncher having the smallest aperture. This allows for better control of the already somewhat focused beam, while also working as a pumping barrier [17, 25].

In order to keep the gas pressure constant in the cooler, gas is constantly fed into the buncher. Mostly the gas escapes through the apertures in the front and end of the device. In the beamline, however, a low pressure is required, and thus the gas needs to be pumped out. Since the rate of gas flow through a lens is dependent on the size of the aperture [17, 25], a lens with a small aperture blocking most of the transverse plane keeps much of the gas between the closest lenses and the buncher, from where it can be pumped away.

4.2.4 Creation of bunches having short temporal spread

The ions entering the buncher have a wide range of transverse positions, directions and energies. To extract narrow bunches from the device, the spread of motion and energy needs to be reduced, which is achieved with the use of the buffer gas. As the ions collide with the buffer gas, they lose much of their kinetic energy and eventually end up at the axial and radial minimum, finally reaching a thermal equilibrium with the gas with some motion added by the Coulomb interaction and the motion induced by the time-dependent radial potential. As the transverse size of the beam decreases, the buncher can also reduce the transverse emittance of a beam.

The temporal spread and the width of the energy distribution of the extracted bunch is largely determined by the remaining motion of the cooled ions, while the amount of ion-gas collisions also play a role [31]. Examining the motion of the ions at the axial minimum can reveal the root cause for the distribution widths.

4.2.5 Motion of cooled ions

Due to the remaining kinetic energy of the cooled ions, they don't lie still at the axial minimum. Just before extraction some ions are located behind and some in front of the minimum, meaning that the ions further back have to cover more distance to get to any transverse plane [31]. Additionally, as the potential during extraction is a descending slope, the ions further back receive more kinetic energy. The shape and depth of the minimum before extraction can thus be used to define how far the from the minimum the ions can be, and the slope during extraction then determines the difference between the energy gain of the ions that are furthest apart. Since the ions obtain different amounts of kinetic energy during extraction, it is clear that the length of the released bunch evolves over time.

First, the bunch reaches the time-focus plane and then it begins to elongate [31]. The time-of-flight distribution is at its narrowest at the time-focus plane, where the faster ions pass the slower ones. Since the energy distribution stays constant, the width of the bunch continues to increase after the time-focus plane. The location of the time-focus plane can be moved by changing the slope of the extraction potential and the voltages on the extraction optics, with steeper potential gradient moving the plane closer to the buncher [31].

The axial minimum cannot be arbitrarily deep however, as the Mathieu parameters

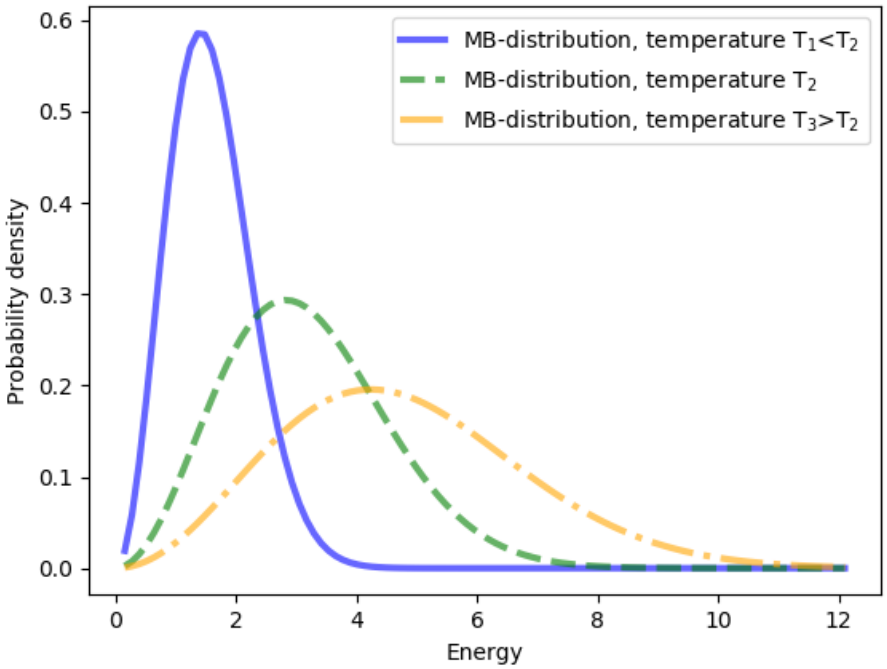

Figure 13. Maxwell-Boltzmann distribution of the same gas at different temperatures. At higher temperatures there are more particles with higher kinetic energies.

can move out of stable positions, which in this case is seen as increased radial motion. While the radial position and motion of the ions during extraction doesn't play as big of a role in the width of the distributions, it affects the transmission of the device and the transverse emittance of the beam. Ions far from the axis are prone to colliding with obstacles and experience greater bending when passing through a lens. As the cooled ion cloud in a buncher behaves much like a gas with motion in all three dimensions, it is often convenient to express the amount of motion using temperature.

4.2.6 Temperature of a bunch

Temperature is the average kinetic energy of an ensemble of particles, and thus the most useful measure for the temperature is obtained from the accumulated ions that have little coherent motion. It is difficult to measure the temperature of just the ion cloud in the buncher, although there are methods to determine the axial temperature from the width of the ToF distribution [32]. Since this work is solely simulations,

the temperature of an ion bunch is deduced numerically.

As per the kinetic theory of gases, gas particle velocities follow the Maxwell-Boltzmann (M-B) distribution [16], the shape of which depends on the temperature of the gas and mass of the particles. Although the velocity distribution of the ions doesn't exactly follow the M-B-distribution due to Coulomb interaction and the motion induced by the time-dependent electric field [17, 23], the difference is negligible and the temperature of the ion cloud can be calculated using the mean energy of the M-B-distribution [23]

$$\langle E_k \rangle = k_b T, \tag{16}$$

where k_b is the Boltzmann constant and T is the temperature, although often the temperature is indicated using just the mean energy. Example of the effect of temperature on the M-B-distribution can be seen in figure 13.

An ion bunch is usually cooled to sub eV energies, i.e. relatively close to room temperature, after which it is be extracted from the buncher. The final temperature of the ions is mainly defined by the temperature of the buffer gas, but also by the induced motion and charge repulsion which both increase the temperature [17]. The temperature of a bunch is therefore always somewhat higher than the ambient temperature. The time the ions need to achieve thermal equilibrium depends on the energy of the injected beam, the gas pressure, and the mass difference of the gas and ion particles [25, 26]. The interaction between an ion and gas can be explained with the use of a gas model.

4.3 Gas models

The inert and charge-neutral buffer gas is an integral part of the function of an RFQ cooler-buncher [10, 19]. The purpose of the gas is to cool the injected ions to reduce their energy distribution so that they can be extracted from the buncher in a tight bunch. The cooling mainly occurs through elastic collisions between the ions and the gas [19, 23]. A light gas compared to the ions must be used in order for the cooling effect to occur [17]. The net result of the collisions is the reduction of the ion's kinetic energy and the ions collect in the axial potential minimum [17, 25]. Without the gas and the cooling it provides, the ions injected into the buncher wouldn't lose their energy, and as such their position and velocity distributions during extraction

would result in enormous temporal spread and energy distribution. The presence of a gas has also been shown to reduce the effect of the unideal potential caused by e.g. misaligned electrodes [19]. As many experiments involve a particle moving in a gas, multiple ion-gas interaction models have been devised to model the interaction.

When choosing a gas model to use, it is important to consider the environment in which the model is used. A simple division can be made based on the pressure domain in which the model is applicable. Historically, the models have usually taken a more averaging approach to collisions, while with increasing computing power, models simulating individual collisions have become widely spread. Still, the number of collisions quickly increases with pressure, as the mean free path decreases, leading to unreasonably long calculation times when modelling individual collisions. On the other hand, as pressure decreases, the amount of collisions per second also decrease and individual collisions play a greater role, and so the predictive power of the averaging models diminishes. Thus models simulating individual collisions are typically used in low pressures and averaging models are used in high pressures [19, 26, 33]. The averaging models are characterised by smoothly decaying motion, while the individual collision models are distinguished by sudden changes in the direction of the ion caused by the individual ion-gas collisions which can also increase the ion's energy [26]. These two types of models are illustrated in figure 14. In this work, a hard sphere model simulating individual collisions was used. In the following sections, a drag model and the hard sphere model are presented.

4.3.1 Drag model

A drag model describes the interaction between the ions and the gas as a particle moving through a viscous fluid. In the model, the ions moving through the gas experience a force opposite to their velocity as [26]

$$\mathbf{F} = -m\beta\mathbf{v}, \tag{17}$$

where v is the velocity vector, m is the mass of the ion, and β is the linear damping coefficient, which in turn consists of [26]

$$\beta = \frac{q}{m\mu} \cdot \frac{p/p_N}{T/T_N}, \tag{18}$$

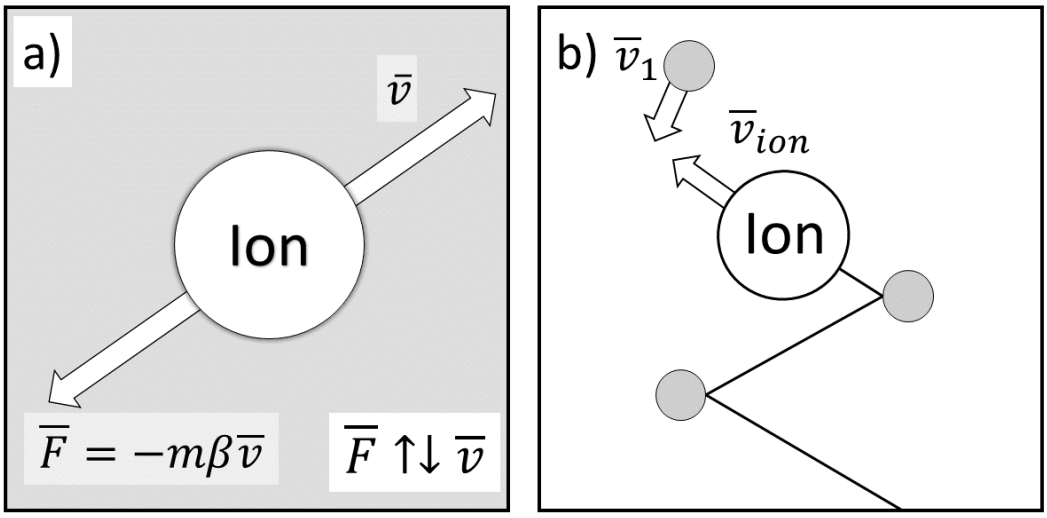

Figure 14. a) In the drag model, the interaction between an ion and the gas is modelled as a force opposing the ion's motion. b) In the hard sphere model, the gas and an ion interact through elastic collisions, which can change the kinetic energy and direction of the ion. The gas particles are not assumed to be stationary.

where μ is the reduced ion mobility, and p/p_N and T/T_N are are the pressure and temperature as fractions of normal pressure (101325 Pa) and temperature (293,15 K). The reduced ion mobility is a constant that depends, among other things, on the velocity, mass and charge of the ion. In the case of light buffer gas particles, it is possible to derive an analytic solution to the equations of motion of an ion in a buncher with the added linear drag model. The stability diagram for the Mathieu parameters in this case shows an enlargement and a shift of the regions of stability, when compared to vacuum conditions [19].

The main benefits of this model are that it is easy to understand and implement, and the fact that an analytic solution exists makes it possible to study the effects of the gas. On the downside, the model assumes that a force exactly opposing the motion is applied to the ions constantly, which especially in low pressure environments doesn't hold. Also, the linear damping constant in this model has an experimentally obtained value, that is dependent on various factors. Since the experiments involving the buncher often contain ions with no known value for the damping constant, great care must be taken when deciding on the value used. The damping constant of an

ion with similar size and mass can be tried instead.

When considering the applicability of this model in a simulation, the time step of the simulation and the mean free time, i.e. the mean time between ion-gas collisions, can be compared. As the drag force is applied on every time step of a simulation, a mean free time longer than multiple steps could lead to unreasonable reduction in the ions' velocity, as drag force would be applied even though no collisions would have occurred. This effect could be reduced by using a lower damping coefficient. Additionally, in the case of a long mean free time, the ion experiences only a few collisions within a time step or none at all. As such, it is unlikely that the total force caused by the collisions on the ion within a time step would be opposite to its velocity, as is assumed by the model. In such case, a hard sphere model taking each individual collision into account can be used.

4.3.2 Hard sphere model

In the hard sphere model used in this work, individual collisions between the ion and the gas atoms are modelled. The model assumes that all collisions are elastic and that these collisions are the only interaction between the gas and the ions. Additionally, the velocity of the buffer gas is assumed to follow the Maxwell-Boltzmann distribution, and the collisions with the ions don't change the shape of the distribution i.e. the gas doesn't warm up or cool down. On the other hand, the ions can either gain or lose kinetic energy at each collision, and the colliding gas particle can come from any direction. Finally, the model assumes that only a single collision can occur within a time step, but this is remedied by the use of an adjustable time step.

The collision algorithm works by taking a random number between 0 and 1 from a uniform distribution, and checking if the number is smaller than the collision probability [28]

$$P = 1 - e^{-v_{rel} \cdot dt/\lambda}, \tag{19}$$

where v is the velocity of the ion, dt the time step, and λ the effective mean free path. If the random number is smaller than the probability, a collision occurs. It can be seen from the equation that with decreasing mean free path, e.g. increasing pressure, the probability of a collision at each time step increases. As the probability of a collision increases, it becomes more probable that there would have actually been more than one collision within a time step. In order for the assumption of one

collision per time step to hold, the size of the step must then be reduced. In the program used in this work, the time step is adjusted so that a collision occurs on average every ten steps, with the length being recalculated whenever a change in pressure or a large change in velocity has occurred.

The mean free path of the ion is calculated using [28]

$$\lambda = \frac{1}{\sigma n}, \tag{20}$$

where v_{ion} is the speed of the ion, v_{rel} the mean relative speed between the ion and the buffer gas, n the number density of the gas, and σ is the collision cross section, the cross section used here is the area of a circle with a diameter being the sum of the colliding gas particle and the ion. As n is the number density of the gas, the ideal gas law can be substituted in the form [16]

$$n = \frac{P}{k_b T}, \tag{21}$$

which leads to a mean free path of [28]

$$\lambda = \frac{k_b T}{\sigma P}. \tag{22}$$

This leaves only the relative speed to be solved.

To get the mean relative speed, a three dimensional integral [28]

$$v_{rel} = \int\int\int_V |\mathbf{v}_{ion} - \mathbf{v}_{gas}| \left(\frac{m}{2\pi k_b T}\right)^{\frac{3}{2}} \exp\left(-\frac{m\mathbf{v}^2}{2k_b T}\right) d\mathbf{v}_{gas}, \tag{23}$$

where m and $\mathbf{v}$ is the mass and velocity of the gas particles, and $|\mathbf{v}_{ion} - \mathbf{v}_{gas}|$ the speed between the ion and a gas particle needs to be solved. Using the assumption that the velocities of the ions follow the Maxwell-Boltzmann distribution, after evaluating the integrals, the expression simplifies to [28]

$$v_{rel} = \overline{v}_{gas}\left((s + \frac{1}{2s})\frac{\sqrt{\pi}}{2}\mathrm{erf(s)} + \frac{1}{2}\exp(-s^2)\right), \quad s = \frac{v_{ion}}{v^*_{gas}} \tag{24}$$

where erf is the error function, $\overline{v}_{gas}$ is the mean gas speed [28]

$$\overline{v}_{gas} = \sqrt{\frac{8k_b T}{\pi m}}, \tag{25}$$

and v^*_{gas} is the median gas speed [28]

$$v^*_{gas} = \sqrt{\frac{2k_bT}{m}}. \tag{26}$$

In the algorithm, the collision kinematics are calculated in the reference frame of the gas particle. Since the velocity distribution of the gas is Maxwellian in the reference frame of the buncher, the velocity distribution of the gas particles that collide with the moving ion is not exactly so, as e.g. a particle moving slower than the ion in the same direction cannot collide with it. It is important to note that in a Maxwell-Boltzmann distribution the velocity is isotropically distributed.

To pick the velocity of the colliding gas particle, a rejection sampling method is used. Using this method, gas particles with lower relative velocity are less likely to collide with the ion. In the method, the velocity of the gas particle is picked from the Maxwell distribution. The magnitude of the relative velocity between the ion and the particle is then scaled (divided) with an approximate upper bound of the relative speed

$$S_c = v_{ion} + 3\sigma\sqrt{3}, \tag{27}$$

where $3\sigma\sqrt{3}$ is three standard deviations of the gas velocity in three dimensions. The three sigmas limit comes from the fact that as the velocity in each dimension is normally distributed, nearly every ion has a velocity lower than the mean plus three standard deviations. The scaled magnitude is then compared with a random number between 0 and 1 taken from a uniform distribution. If the scaled magnitude is less than the random number, the velocity is rejected and a new value from the Maxwell distribution is picked. This continues until the scaled velocity is greater than the random number.

After a suitable velocity is found, the collision kinematics are then calculated as a usual two body elastic collision between two spheres, where the spheres don't necessarily have to collide head on. As a result of the collisions, the velocity distribution of multiple ions becomes nearly Maxwell distributed at equilibrium with the gas. Compared to the drag model, hard sphere models are commonly thought to produce more accurate results at low pressure environments [26] and so the hard sphere model described above is used in this work.

5 Software

The design process of the buncher was done using three programs, Autodesk Inventor, a 3D computer aided design (CAD) software, SIMION, an ion optics simulator, and SIMION SLTools, a program used to import the geometry designed in Inventor to SIMION. In addition, some Python scripts were written and modified by me to help with running the simulations and analyse the results. The workflow in using these programs was the following: first the geometry of the buncher was designed using Inventor, then the geometry was imported into SIMION using the SLTools program, and finally ions flying through the geometry were simulated using SIMION. This process was then repeated until a geometry and operating parameters resulting in small temporal and energy spread and high transmission were found. In this chapter, a short description of each program is given with a more detailed explanation on the workflow presented in the appendix A.

5.1 SIMION

SIMION is the ion optics simulator at the heart of this work. As the name implies, the program is used to simulate the three dimensional trajectories of ions in electric and magnetic fields, although only electric fields are used in this work. The version 8.1.1.32-2013-05-20 of SIMION was used in this work.

To be able to simulate the ions, the electric potential inside the desired volume must be known. To calculate the potential in the system, SIMION divides the simulated volume into a point grid, where each point either belongs to an electrode or is empty space. The voltage of each electrode can be set separately in the program and the electric potential caused by the electrodes at each grid point is calculated using an over-relaxation finite difference method to solve the Laplace equation [34]

$$\nabla^2 \phi = 0, \tag{28}$$

where ϕ is the electric potential. The electric potential is calculated separately for each electrode as due to the nature of the equation, the potential at each point is the

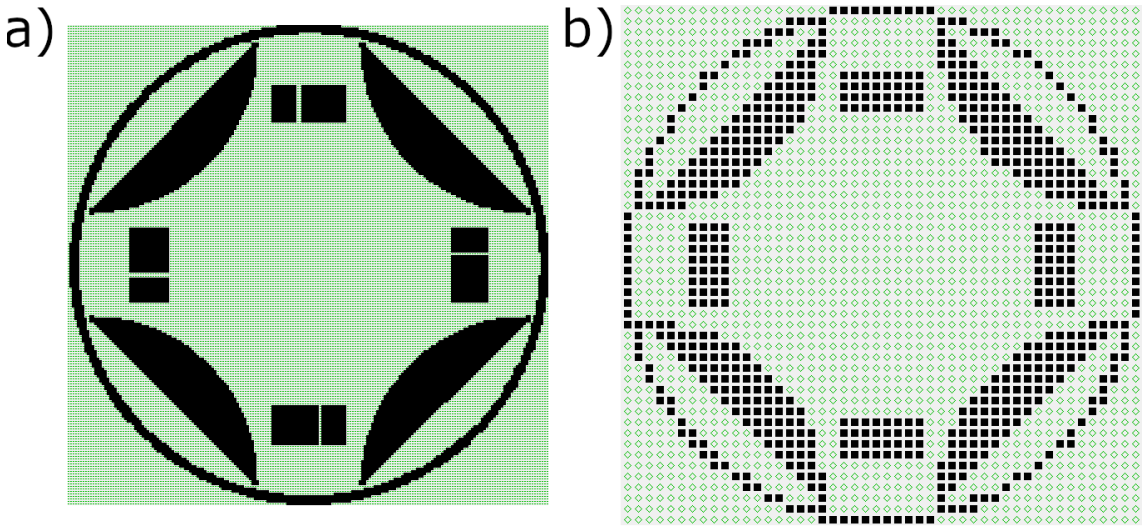

Figure 15. A cross section of the buncher main section, where different grid point densities were used. The black squares represent electrodes, while the green diamonds are empty space. Using the denser grid in a), the round shape of the RF rods is conserved better. As the electric potential is calculated at every empty point and the potential between the points is interpolated, a denser grid results in more accurate representation of the potential.

sum of the potential from each electrode and the potential caused by an electrode scales with the applied voltage. This makes it possible to change the electrode voltages during simulation without calculating the potentials again [34]. While it is possible to create the electrode geometries in SIMION, it is much easier to design the geometry in a separate modelling software, e.g. Autodesk Inventor, and import the model to SIMION using the SLTools program that comes with SIMION.

In the known electric potential, SIMION calculates the ion trajectories using the fourth order Runge-Kutta method [35] to solve the differential equations of motion resulting from the Lorentz force [34]. During simulation, the electric potential experienced by the ion is interpolated using the potential at the nearest grid points. It is possible to simulate the ions one by one so that they don't interact with each other, or in a grouped fly mode, where the ions can be set to experience Coulomb repulsion. The grouped fly mode can thus be used to simulate the space charge effect.

As the Coulomb force needs to be calculated for every pair of ions on every time step, the number of particles that would need to be simulated to have a meaningful repulsive effect is too high for most cases. For this reason SIMION has an option to set the strength of the repulsion. This way a single simulated particle can be

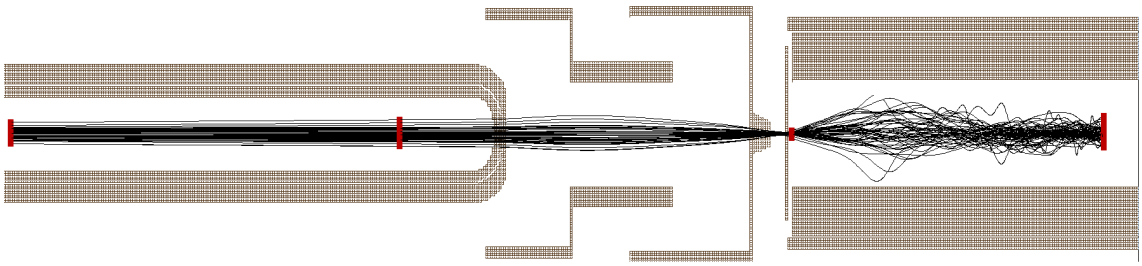

Figure 16. A side view of the injection optics in SIMION. The black lines are ion trajectories and the red squares are locations where the ions' properties, such as velocity, are recorded.

used to represent any number of real ions, although using too few simulated particles leads to less accurate results. The interaction between the simulated particle and the electric field of the electrodes is then handled as if the particle had a mass and charge of a single real ion, but the Coulomb interaction between the particles are handled as if the particles had the mass and charge of a single ion times the number of ions the particle represents [34].

The charge repulsion method in SIMION is simplified so that the ions don't affect the charge distribution on the electrode surfaces, as this would mean that the electric fields from the electrodes and the ions are coupled. Calculating the coupled electric fields would require solving the Poisson equation on every time step, which would be prohibitively expensive computationally. Simulations using the repulsion are thus less accurate the more time the ions spend close to electrodes [34].

The parameters that affect the quality of a simulation the most is the density of the point grid and the size of the time-step in the Runge-Kutta algorithm, with denser grid and shorter time-step resulting in more accurate simulation. An example of the model using two different grid densities is shown in figure 15. The grid, however, cannot be arbitrarily dense as the whole grid needs to be loaded into the computer memory, which can quickly run out. A similar limit is set on the length of the time-step, as a small-time step can lead to prohibitively long simulation times. While SIMION itself is not parallelised, meaning that the calculations are done only on one processor core, it is possible to run multiple instances of SIMION simulating the same volume with the same parameters. This can be used to simulate more ions in a given time if more cores are available, but the amount of required memory is multiplied by the number of instances.

In the program, it is possible to set the properties, such as the mass and charge,

and initial values, such as initial velocity and position, of the ions. SIMION also allows the user to write so-called user programs that can access all the information available in the simulation using the lua programming language. The programs can be used to, for example, change the voltages of electrodes, simulate the effect of a background gas, compute properties of the beam and run a series of simulations with different parameter values, just to name a few applications used in this work. Finally, the properties of the ions, such as velocity, can be recorded at any point. A picture of a typical simulation is shown in figure 16. Instead of creating the geometry used in this work in SIMION, a dedicated geometry modelling software Autodesk Inventor was used.

5.2 Autodesk Inventor

Autodesk Inventor is a 3D CAD software. The program can be used to create three dimensional shapes called parts and multiple parts, or multiple instances of the same part, can be arranged in a desired fashion into an assembly. In this work, Inventor was used to design the geometry of the electrodes in the buncher, which includes designing the shapes of the electrodes and their placement in the buncher. Autodesk Inventor Professional 2020 was used in this work.

In Inventor, each differently shaped electrode is its own part which are then put into an assembly where the relations, i.e. distances and angles, between the parts are fixed to form the desired geometry. As SIMION uses each instance of a part as a single entity and, for example, the voltages are set on a per part basis, it is possible to improve the performance of the simulations by noticing that the buncher contains lots of symmetries. Since the opposing RF rods in a buncher always have the same voltage, the opposite rods can be made into a single part. Similarly the four DC wedges facing the same direction can also be made into a single part. To use the created geometry in SIMION, the assembly must be exported from Inventor and converted into a format SIMION can work with by using the SLTools program.

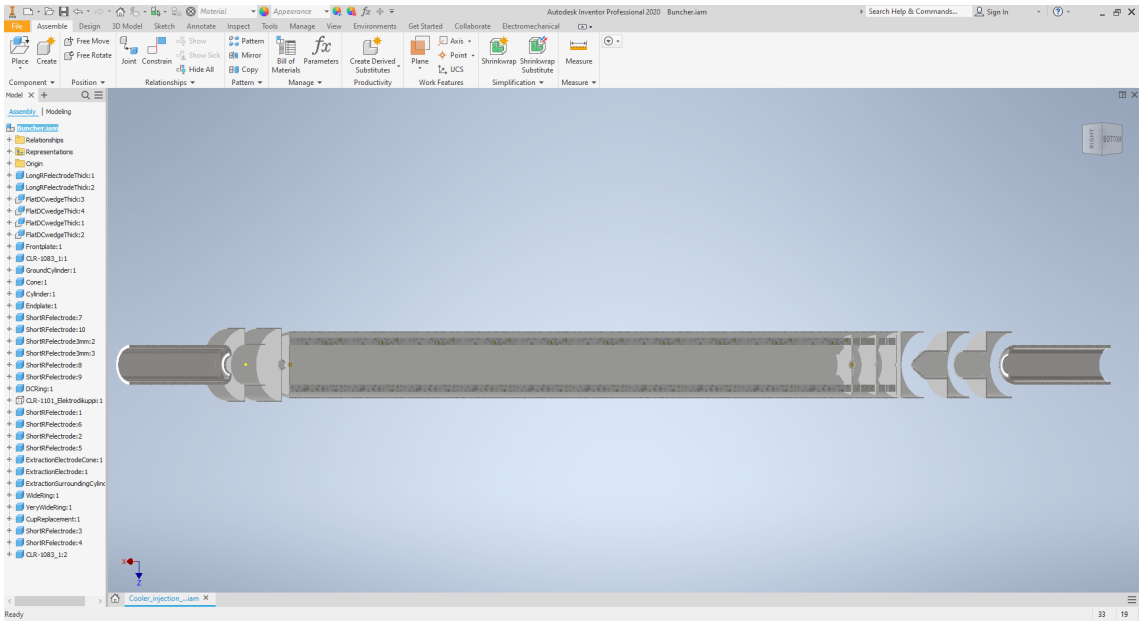

Figure 17. A view of the buncher (centre), and the injection (left) and extraction optics (right) in Autodesk Inventor.

5.3 SLTools

The SLTools program was used to create the point grid used by SIMION based on the geometry designed in Inventor. The most important feature of this program was the ability to select a section of the geometry to turn into a point grid. This feature was very useful, as simulating ions in the whole buncher volume with a reasonably dense point grid would have required more computational power than was available. SLTools comes packaged with SIMION, and as such doesn't have its own version number.

5.4 Custom scripts

In addition to the professional programs, some self made or modified lua and Python scripts were used in this work. The essential scripts used were the SIMION user program that handled the actual operation of the buncher and the gas collision file that SIMION used to calculate the hard sphere ion-gas collisions. In addition, I wrote various Python scripts to analyse the data obtained from the simulations and create the data figures shown in chapter 6.

While the gas collision file comes packaged with SIMION, it was modified by Marc Schuh [36], and some modifications were also done by me. Using this file, the

parameters of the model could be set, such as the gas pressure at different parts of the buncher, which was made easier by my modifications.

The user program was created by Marc Schuh [36], modified by Antoine de Roubin, and further modified by me to suit this work. The main purpose of the user program script was to control the voltages of the electrodes. It was possible to set static voltages, alternating voltages of any time structure, and switch voltages at a given time. Three major additions to this file were made by me, the first of which was the ability to run a series of simulations with predetermined operational parameters, such as electrode voltages, and recording the resulting transmission efficiency, and time-of-flight and energy distributions. This feature was regularly used to scan a range of values for a parameter, for example, to find parameter values minimising the width of the ToF distribution.

Another addition was the possibility of reading the initial values, i.e. position, velocity and time-of-flight, for ions from a file. This was useful, as the whole buncher couldn't be simulated at an acceptable resolution of the point grid, and as such was split into four segments with better resolution. Using this addition made it possible to record the position, velocity and time-of-flight of the ions at the end of one segment and initialise them in the following segment with the same values.

The final addition was the possibility of initialising the ions so that the beam had a given transverse emittance. This addition was needed in order create injected beams with a given transverse emittance. The code makes it possible to change the Twiss parameters to obtain beams of different properties. The distribution of ion positions and initial directions in this method is Gaussian. Using these programs, it was possible to create the geometry for the buncher and the injection and extraction optics, and evaluate their performance.

6 Results

In this work, the geometry for a RFQ cooler-buncher and the injection and extraction optics was designed, and the design's performance was evaluated using SIMION to simulate ions flying through the design. The designed geometry consisted of the electrodes intended to manipulate the ions and didn't include the supporting structure. The goal was to bunch a continuous ion beam of 5 keV of kinetic energy and 17 π·mm·mrad transverse emittance and obtain bunches with short temporal spread and small energy distribution, while maintaining high transmission. The geometry presented in this chapter was the results of tens of iterations, where the amount of electrodes and their shapes and positions were modified to find a well performing geometry. The geometry was designed in three segments, the injection optics, the main RFQ section, and the buncher extraction composed of the bunching sections and extraction optics. The split allowed to concentrate on one segment at a time to perfect its performance. As each segment of the buncher serve a different purpose, different characteristics were used to evaluate the performance of the segments during the design process.

High transmission was a major goal for each segment, while also the degree of cooling was important for the main section and the extraction. As the extraction was the last segment the ions flew through and it has the greatest effect on the quality of the bunches, the width of the time-of-flight and energy distributions at the end of the segment were a major indicator of its performance. The performance of a segment could be changed by altering the device geometry, i.e. the shape, size, and position of the electrodes, or by adding new ones. In addition to the geometry, proper values for the operational parameters, such as the gas pressure, electrode voltages and RF frequency, needed to be optimised to obtain the best possible results. After the performance of each individual segment was sufficient, ions were simulated going through the whole design and the geometry and parameters of the segments were adjusted if necessary.

In this chapter, first the geometry of the buncher is described and the motivation behind some of the design choices are presented. Then, the simulation process is

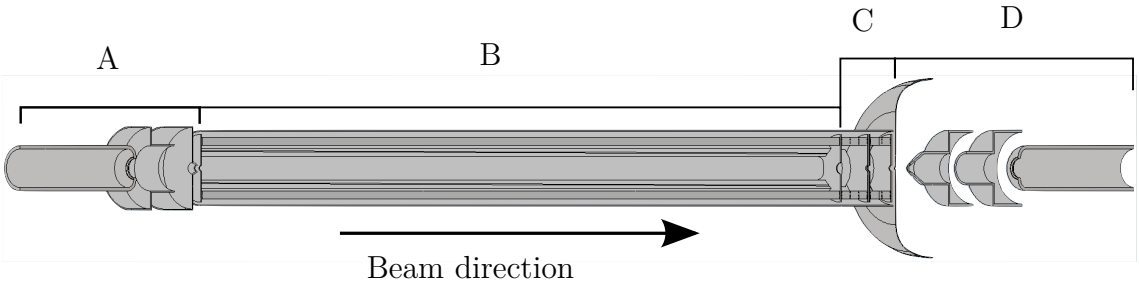

Figure 18. The geometry of the buncher designed in this work. Only the electrode surfaces exposed to the optical axis are modelled. The injection optics (A) focus the incoming beam into the main RFQ section (B). In the main section the ions are cooled while being transported to the bunching sections (C). The extraction optics (D) are used to focus the extracted ion bunch to arrive at the subsequent devices in the beamline.

presented, and finally the results of simulations done using the geometry are presented. These include a simulation using the optimal parameter values to determine the best possible performance, and simulations where some operational parameters or the ion type were changed and the effect on the results observed.

6.1 Geometry of the designed buncher

The finalised geometry of the buncher is presented in figure 18. As the goal of the work was to simulate ions flying through the buncher, only the elements and surfaces that are exposed to the volume where the ions move were modelled to speed up the design process. This means that the parts are "hovering" in the model, as support structures, metallic or dielectric, were not included. As the metallic support structure and wires are in some potential, and dielectrics can become charged, they can alter the electric potential inside the buncher. Although the support structure and wires were not modelled, the effect of the stray fields was considered by designing the geometry so that as little of the support structure would be exposed to the volume as possible.

Additionally, to prevent electrical discharges from breaking any equipment, effort was put into spacing electrodes that are set to different potentials. A spacing of 1 mm per 1 kV of voltage difference was used as a rule of thumb, although the actual minimum spacing before a discharge depends on the geometry of the electrodes, the type of gas and pressure, among other things [17]. The electrodes in the model contain many sharp corners that will be rounded in the actual device to also minimise

the chance of electrical breakdowns [17]. As the electrodes in SIMION are represented by a square grid that is too coarse to capture the smooth edges, no smoothing was done.

To see whether the wedge electrodes could be used to create a potential transporting the ions through the buncher, while also cooling the ions, the main RFQ section was designed first. After the main section, the injection optics were designed, as this would allow testing the bunching section with a realistic injected beam. Lastly, most time was spent designing and fine tuning the bunching sections and extraction optics, as these have the greatest impact on the quality of the bunches.

6.1.1 Main RFQ

The main section consists of four round RF rod, eight DC wedge and two plate electrodes. The rods are placed in a circular pattern around the axis, while a pair of wedges facing the opposite directions are placed in each of the four gaps between the rods. The main section is presented in figure 19, along with the most important dimensions and names of the electrodes.

According to the simulations, the length of the main section allowed the ions to cool sufficiently. When compared to other bunchers, the distance from the axis to the electrodes is on the upper end of the spectrum [25, 37]. This is to allow room for placing the wedges between the rods, as the wedges couldn't realistically be made any thinner, due to their attachment method. The thicker end of the wedges could be made narrower, but the current arrangement seemed to produce good results, and getting the rods closer to the axis thus isn't mandatory. The downside of having the rods far away is that a higher amplitude, going up to kV-range peak-to-peak, needs to be applied to confine the ions, but producing such a voltage shouldn't be a problem and all the electrodes are spaced so that electrical breakdown shouldn't occur. On the flip side, larger volume allows for more ions in the buncher without decreasing the transmission, as the quadrupole approximation of the radial potential is valid further from the axis allowing ions to be further from the axis, thus making it possible to confine more ions before the space charge effect becomes an issue.

Since the main RFQ section is filled with buffer gas, the purpose of the injection plate, V_3 in figure 20, is to keep the gas inside the buncher but allow the beam to enter. On the other hand, some gas is supposed to enter the bunching section, so the aperture in the plate separating the main and bunching section, V_4 in figure

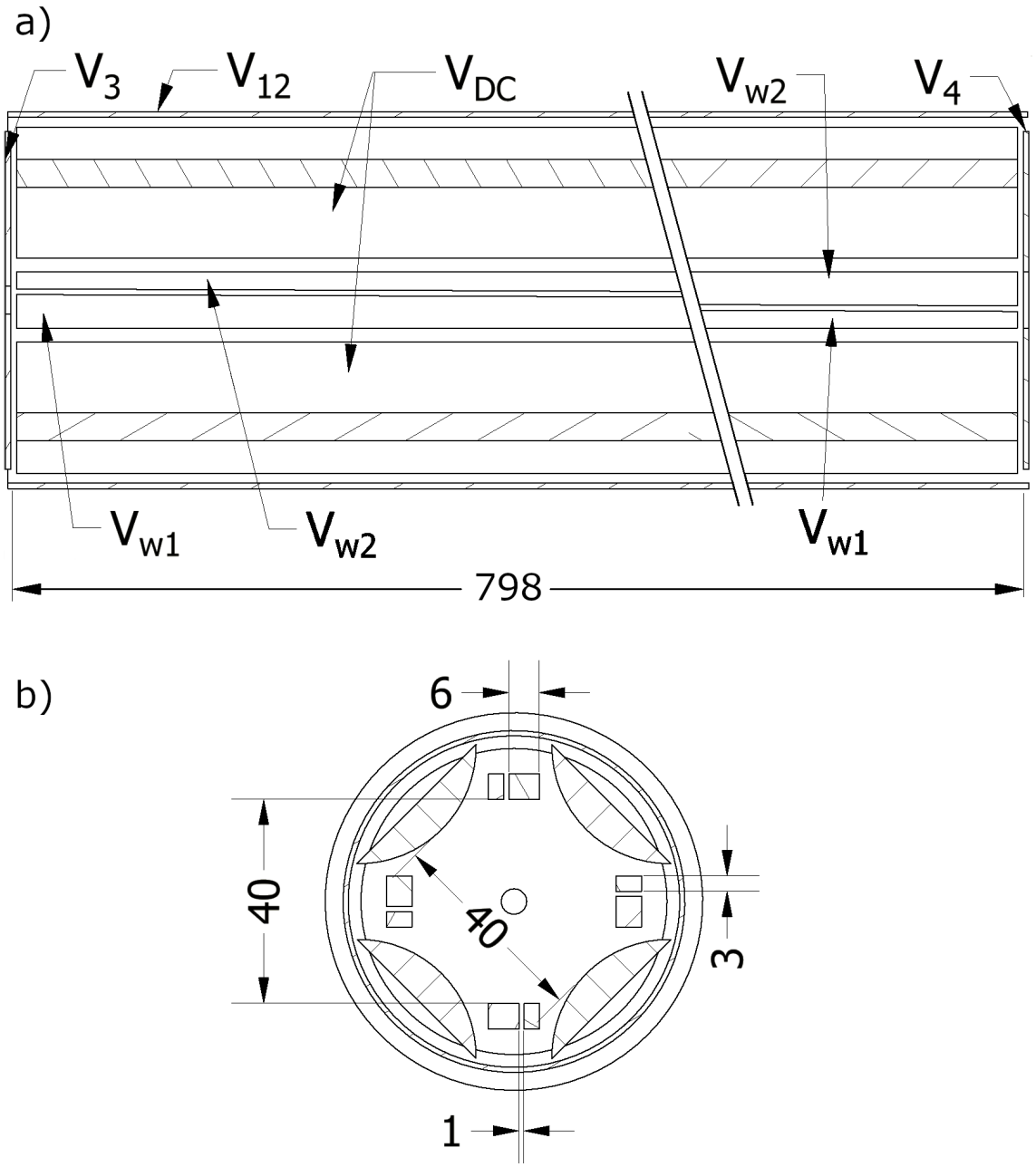

Figure 19. a) A side view of the main RFQ section, with b) a cross section at the end of the device. Some important dimensions are indicated in millimetres. The voltages corresponding to the named electrodes can be found in table 1.

20, is larger than on the other plates. In the simulation model a hollow cylinder encloses the main section representing the high voltage chamber the device sits in. The chamber in the actual structure is larger, but the cylinder was used as the smaller size sped up the simulations and shouldn't affect the results. After the main

section was found to work well, the injection optics were designed to test whether main section could confine a poor quality beam.

6.1.2 Injection optics

The injection optics consist of three electrostatic aperture lenses, shown in figure 20 along with the most important dimensions and names for the electrodes. First the ions enter the ground electrode, V_0 in figure 20, that sets the zero voltage reference for all the other electrodes in the simulations. The ground electrode is followed by two electrostatic lenses that are used to focus the beam through the hole in the injection plate, V_3 in figure 20. The lenses and the plate are also used to lower the beam energy by setting the voltage in the injection plate so that the beam enters the buncher with the desired injection energy and the voltage in the lenses somewhere between ground and the plate voltage.

The apertures in the ground electrode and the first lens are wide as it allows focusing a beam with large emittance. Attached to the lenses are hoods that cover most of the beam's path to the buncher. The hood makes it possible to better define the potential on the axis by preventing the electric potential caused by wires and other objects from reaching the axis. There are large gaps between the electrodes to prevent electrical discharge and to allow for pumping away the gas that escapes from the main buncher section. After a geometry for the injection optics able to efficiently transfer a poor quality beam into the main section was found, a lot of time was used to optimise the performance of the bunching sections by iteratively modifying the geometry and voltages of the components.

6.1.3 Bunching sections and extraction optics

The geometry of the bunching sections and the extraction optics is shown in figure 21, which also includes the names of the electrodes and some of the dimensions. Instead of using a single bunching section, the model uses two sections, the first for accumulating the ions and the second for extracting the bunch. Both sections contain RF rods with same dimensions as in the main section. They are segmented to three to allow for DC potential application for finer control on the axial potential. This choice of dimensions makes it possible to use the same voltage and frequency in the bunching sections and the main section, simplifying the electrical system, especially the RF application. As the rods are quite far away from the axis, the bunching

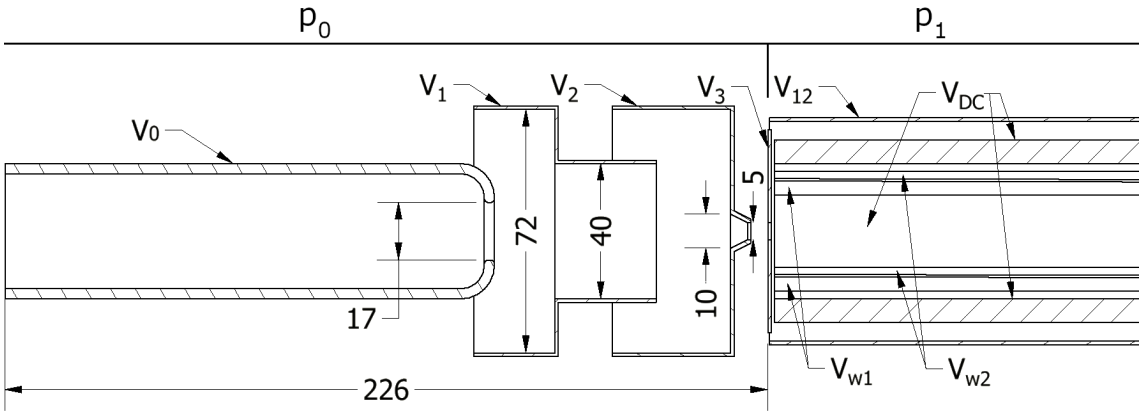

Figure 20. The electrode configuration of the injection optics with some of the most important dimensions indicated in millimetres. In addition, the various electrodes and the two pressure regions are indicated, with the respective voltage and pressure values available in table 1.

sections couldn't be made much shorter as the potential of the plate electrodes started to dominate over the RF on the rods, interfering with the ion confinement and thus leading to reduced transmission efficiency. The large volume of the bunching sections allow containing large amounts of ions, while the short RF rod segments in the second section makes it possible to create a narrow axial potential well.

Between the two sections are two plate electrodes. If only one plate was used between the sections, the ions accumulated in the first section would fly back into the main section during bunch extraction and some would be lost and the rest would need to be cooled again. This two-plate approach ensures that during extraction, the increased voltage of the electrode V_6 in figure 21 doesn't affect the potential in the first bunching section. The plates also prevent too much of the gas from entering the second section.

The bunching sections are followed by the extraction optics, that consists of four electrostatic aperture lenses. The electrodes are used to accelerate the bunches while also focusing the beam to the devices following the buncher. Like the injection, the extraction needs to be in high vacuum but also the potential on the axis needs to be shielded from the effects of stray fields. Therefore, the hood structure is also used with these electrodes.

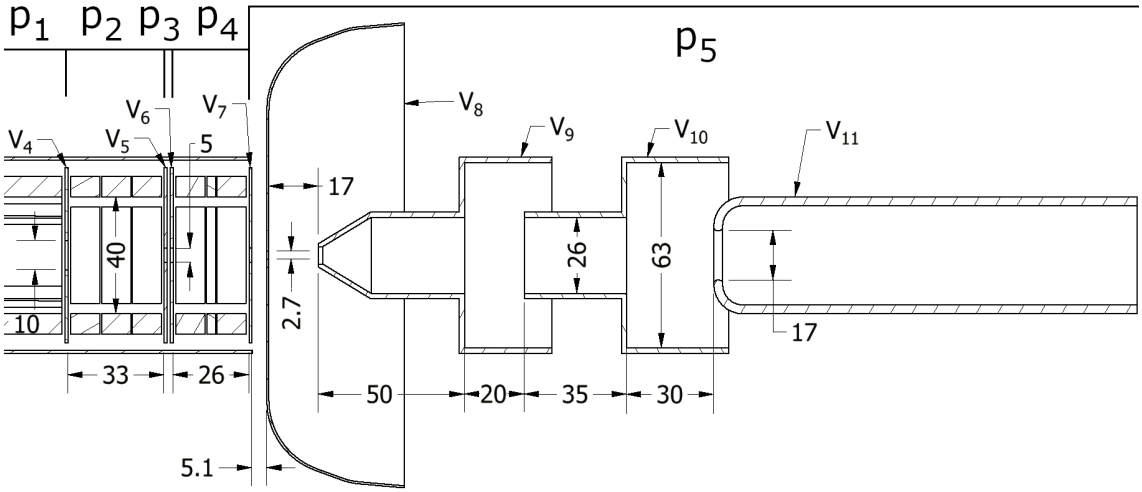

Figure 21. The electrode configuration of the bunching sections and the extraction optics with some of the most important dimensions indicated in millimetres. In addition, the various electrodes and the pressure regions are indicated with the respective names, the voltage and pressure values can be seen in table 1.

6.2 Simulations

For the purpose of the simulations, the design was split into four segments, each simulated separately:

- injection optics, including few centimetres of the main RFQ section,
- main RFQ section,
- first bunching section, including few centimetres of the main RFQ section,
- first and second bunching sections, including the extraction optics.

The split was done as the whole model couldn't be loaded in SIMION at an acceptable resolution, due to the limited available memory. The position and velocity of the ions was saved some millimetres before the end of the simulated volume and the ions could be initialised with these values in the following segment. This way the transfer from one segment to the next could be simulated more accurately, as any possible fringe effects from the simulation boundary could be reduced. Also, the time-of-flight of the ions was recorded and applied when moving from one segment to another, as this way the phase of the RF signal remained consistent and the time-of-flight through the whole design could be recorded.

The third segment was kept short to allow for a denser point grid, leading to a more accurate electric field and trajectory calculations. This was done, as the transfer of ions from the main RFQ section to the bunching section was one of the biggest source of transmission loss, along with the move from the first bunching section to the second.

Although the ion-gas collisions could be simulated using SIMION, the program cannot be used to simulate the flow of gas in the volume. As the geometry was designed so that the buffer gas is fed into the main RFQ section while the injection and extraction optics are kept in high vacuum, the pressure in other parts of the device needed to be determined. To do this, the gas flow was simulated using a gas flow simulation software COMSOL, resulting in the pressure values used in this work (A. Jaries, 2021, private communication).

Finding the operational parameter values resulting in optimal performance was done partly by hand and partly by scanning a range of values for a parameter, such as an electrode voltage and the pressure in a region. In a scan, 200 ions were used to evaluate the performance with a given value, as the total amount of ions quickly skyrockets with the number of scanned parameters and number of steps in the range. As the determination of the bunch widths is more certain for larger amounts of data, 5000 ions were simulated flying through each of the segments to obtain the results shown in this work.

With the computer used in this work, simulating 5000 ions with parameters shown in table 1 took anywhere from two to five hours, with the first and third segments being the fastest due to the faster ions and smaller volume, respectively. As the size of the time step greatly affects the simulation speed, increasing the pressure, and due to the adaptive step size thus decreasing the step size, increased the simulation time. Increased pressure also increased the time it takes for the ions to move through the main RFQ section. A steeper potential gradient in the main section on the other hand resulted in faster simulations. Other parameters didn't have much of an impact on the length of the simulation, except obviously for the cooling time.

Unless otherwise stated in the following sections, the simulation parameters described in this and the following paragraph, and buncher operational parameters presented in table 1 were used throughout the work. Each ion was simulated individually, i.e. repulsion between ions was not modelled. The ions had a mass of 100 u, charge of 1 e, and the hard sphere collision model was used. In the collision

model the buffer gas was assumed to be helium, so a mass of 4 u was used for the gas particles, and radii of 1,4 Å for the helium particles and 3,0 Å for the ions [38]. The temperature was assumed to be 293 K in every segment. Five regions, as shown in figures 20 and 21, with different pressures were used. In the injection segment, the ions were initialised with an energy of 5 keV and a transverse emittance of around 17 π·mm·mrad, with x, x', y and y' being distributed in a Gaussian fashion so that the resulting transverse ion beam profile was cylindrically symmetric. The potential difference between the injection optics and the main RFQ section was such that the ions entering the main section had and kinetic energy of around 100 eV.

The timing scheme of the buncher consists of three phases: accumulation, transfer, and extraction. First in the accumulation phase the ions are allowed to freely drift into the first bunching section, where the minimum of the axial potential is located. Then, after 8000 microseconds since the start the ions are transferred to the second bunching section, from which they are extracted after 1500 microseconds.

In the following chapters, first the results of the simulation using the operational parameters optimised for short temporal spread and high transmission, shown in table 1, are presented, along with the results for a small energy spread. Then, the effect of various key parameters on the performance have been studied. As the optimal performance of the buncher depends on the interplay of all the parameters, optimisation of just a single parameter at a time is not enough to bring the setup to its best performance. Insight is thus needed in the optimisation process.

6.2.1 Performance optimisation results

The goal of optimising the performance of the buncher was to find such operational parameters, that the temporal and energy spread of the extracted bunch was as narrow as possible, and that the transmission through the device was the highest possible. The transverse emittance of the bunch was also of importance. As it is possible to improve some of these qualities at the expense of others, first, the results for short temporal spread and high transmission are presented, followed by results for small energy distribution and high transmission.

Using the operational parameters optimised for small temporal spread shown in table 1, the transmission through the whole device was ∼96 %, and the width of the ToF distribution was 43 ns and energy distribution 30 eV, as shown in figure 22. Most losses in transmission occurred during the transfer from the first bunching

Table 1. The operational parameters of the buncher. A dash indicates that the value is the same as in the previous phase. 20 μs after the transfer phase, the voltages are set to the values in the "accumulation" column until the extraction phase. In V_6, V_7 and V_8, values optimised for small ToF spread/small energy spread are indicated. The corresponding electrodes for the voltages are shown in figures 19, 20 and 21, where also the pressure regions are shown.

	Operation phase		
Parameter	**Accumulation**	**Transfer**	**Extraction**
Phase start time, t	0 μs	8100 μs	9600 μs
Injection ground, V_0	0 V	-	-
1st injection lens, V_1	4400 V	-	-
2nd injection lens, V_2	4100 V	-	-
Front plate, V_3	4900 V	-	-
RF rods, DC, V_{DC}	4880 V	-	-
RF rods, AC amplitude, V_{AC}	500 V	-	-
RF rods, frequency, f_{AC}	500 kHz	-	-
Front facing wedges, V_{w1}	4950 V	-	-
Back facing wedges, V_{w2}	4880 V	-	-
1st bunching plate, V_4	4891 V	4910 V	4891 V
1st segment ring, DC, V_{s0}	4884 V	-	-
2nd segment ring, DC, V_{s1}	4881 V	-	-
3rd segment ring, DC, V_{s2}	4881.2 V	-	-
2nd bunching plate, V_5	4893 V	4884,5 V	4893 V
3rd bunching plate, V_6	4900 V	4884,5 V	5380 V/4905 V
4th segment ring, DC, V_{s3}	4881.5 V	-	-
5th segment ring, DC, V_{s4}	4850 V	-	-
6th segment ring, DC, V_{s5}	4874.2 V	-	-
End plate, V_7	4898 V	4898 V	4838 V/4890 V
Skimmer plate, V_8	4200 V/4800 V	-	-
1st extraction lens, V_9	4166 V	-	-
2nd extraction lens, V_{10}	1666 V	-	-
Extraction ground, V_{11}	0 V	-	-
Surrounding cylinder, V_{12}	5000 V	-	-
Injection pressure, p_0	10^{-6} Pa	-	-
Main RFQ pressure, p_1	2,50 Pa	-	-
1st bunching section pressure, p_2	1,50 Pa	-	-
pressure between the sections, p_3	0.85 Pa	-	-
2nd bunching section pressure, p_4	0,36 Pa	-	-
Extraction pressure, p_5	10^{-6} Pa	-	-

section to the second, while some were also lost during extraction. Additionally, the transverse emittance of the extracted bunch was 9 π·mm·mrad, shown in figure 23,

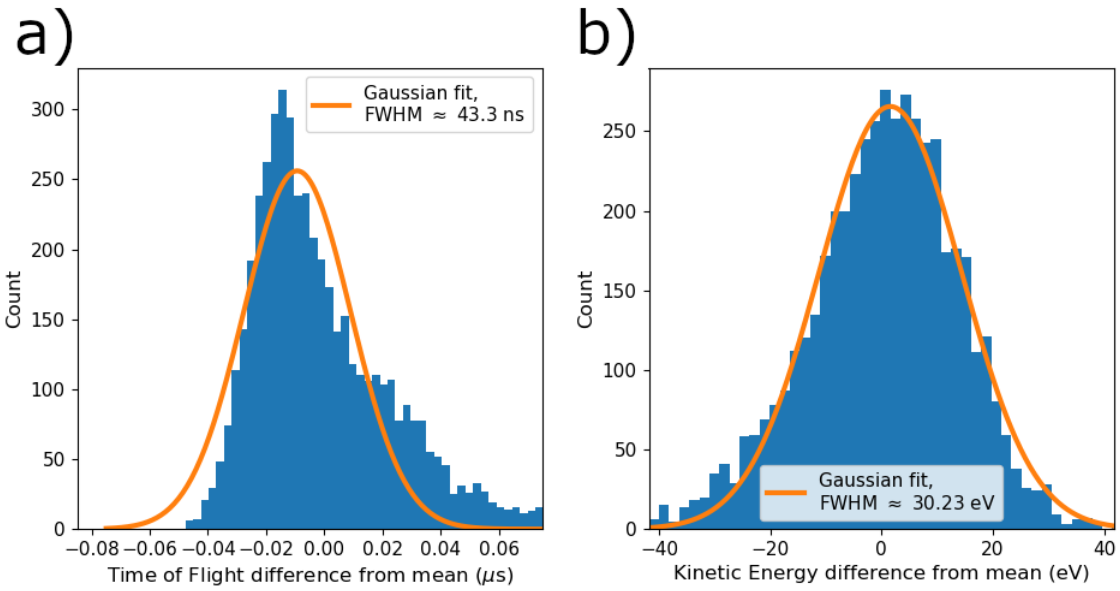

Figure 22. The time-of-flight distribution a) and the energy distribution b) of the ion bunch using the operational parameters optimised for short temporal spread in table 1. Collisions with gas during extraction cause the tail visible in a).

with a kinetic energy of 5 keV. The temperature of the cooled bunch at time $t = 8000$ μs was 1008 K.

The position, velocity and time-of-flight of the ions were recorded in the first bunching section at $t = 8000$ μs. Since in many of the following simulations, the effect of changing some parameter in the second bunching section is evaluated, these same initial ions can be used to form a consistent starting point for the simulations.

While most effort was put into optimising the operational parameters for small temporal spread, some time was spent optimising the extraction potential for bunches with small energy distribution. With the parameters optimised for small energy spread, shown in table 1, the transmission and emittance were similar as before, but the ToF width was 1,1 μs and the energy spread 0,78 eV.

As the operational parameters are chosen so that the data is recorded at the longitudinal focal point before the end of the extraction optics, the parameters given in table 1 are not optimal for a focal point further away. Nevertheless, the results show the achievable widths, and similar results should be obtainable further away by adjusting the parameters of the second bunching section and extraction optics.

Much of the time in each simulation was spent waiting for the slowest ions to make their way into the bunching section, as each simulated ion was valuable due to

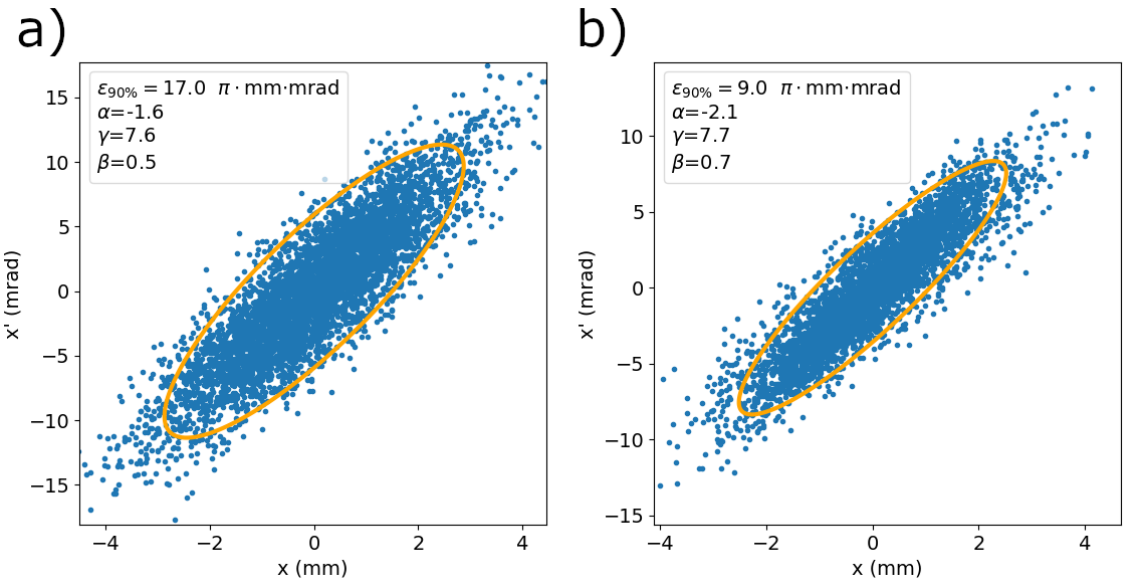

Figure 23. The transverse emittance of the a) injected and b) extracted ion beam, along with the Twiss parameters. In both cases, the beam had an energy of 5 keV.

the time a simulation takes and as the FWHM fitting benefits from a large number of occurrences. The long time the ions took to reach the bunching section is caused by the point grid used to represent the DC wedges in SIMION.

6.2.2 DC wedge electrodes

The wedge electrodes are used to create a DC gradient to allow the ions to flow into the bunching section. Since the wedges are shaped like a tall right triangle, the coarse grid used to represent the volume in SIMION cannot represent the angled side accurately. This results in the slope being modelled as a staircase, illustrated in figure 24 b). This staircase is then also seen in the electric potential in the main RFQ section, as shown in figure 24 a).

Due to the staircase potential, the ions consistently get stuck in the main RFQ section, increasing the time it takes for them to reach the bunching section. Fortunately, the wedges don't affect the potential in the bunching section, and as such don't affect the properties of the bunches. Since the wedges in reality are smooth, it is reasonable to expect that in the actual device this effect is not present and the gradient should be close to linear.

To study the effect of the slope of the gradient, the voltage on the backwards

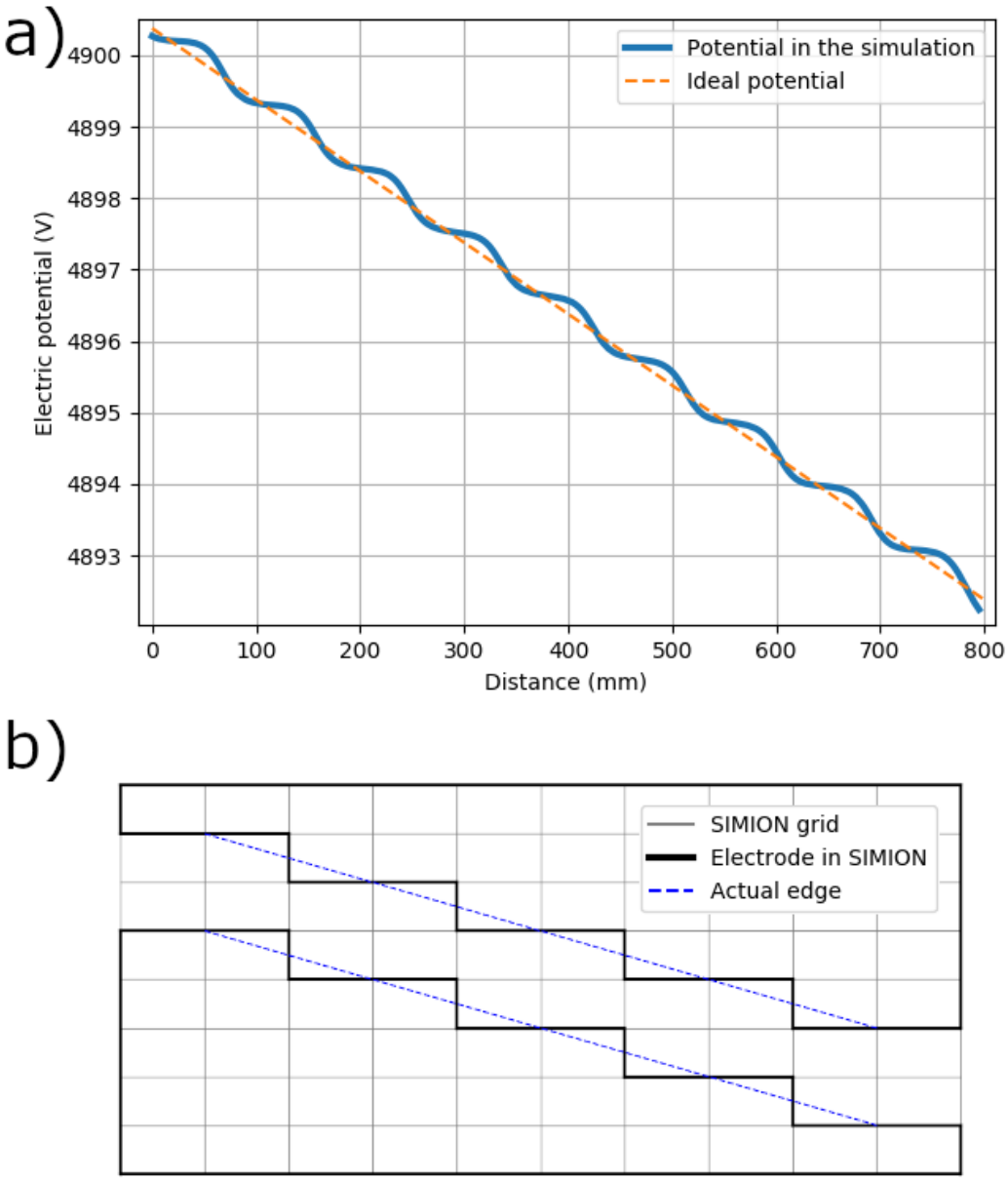

Figure 24. a) The electric potential in the main RFQ section in the simulations, with a difference of 70 V in the wedge electrode potentials. In the actual device the potential should be close to linear. b) The bumpy potential is caused by the coarse point grid SIMION uses to represent the volume and electrodes, as illustrated here. This effect should only affect the time the ions take to arrive at the bunching section. Even with the "staircase gradient" there is always a constant "downhill".

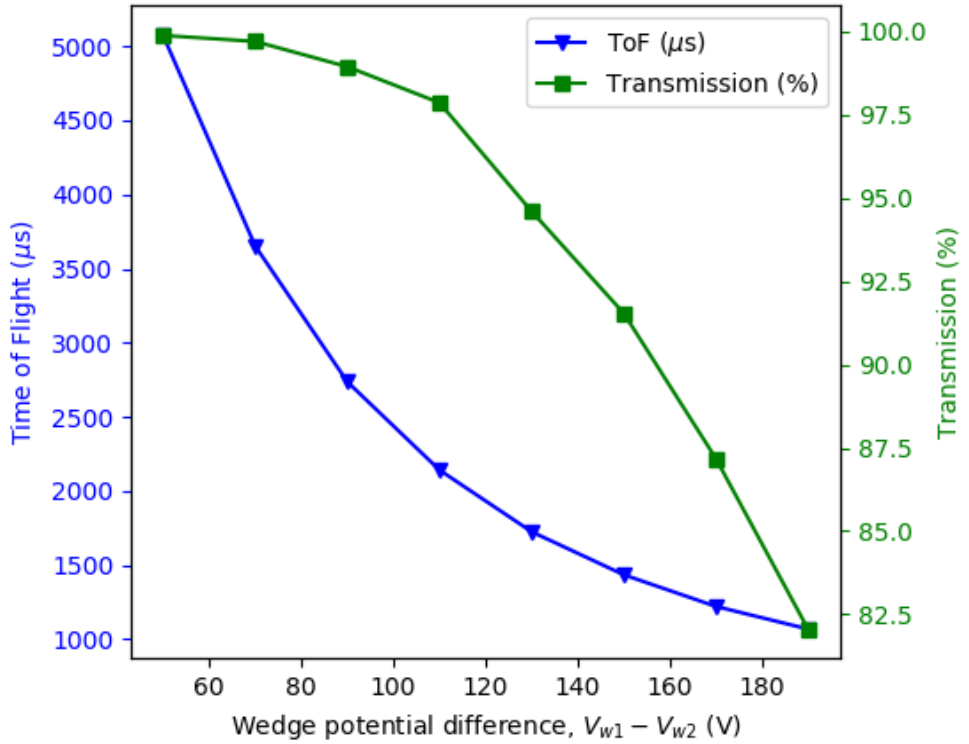

Figure 25. The transmission and time-of-flight of ions reaching the first bunching section at different wedge electrode potential differences, with $V_{w1} = 4950$ V.

facing wedges V_{w2} and the bunching sections was changed. If only the voltage V_{w2} is decreased, the cooled ions don't have enough energy to cross the potential of the plate V_4 in figure 21, effectively killing the transmission. Similarly, only increasing the voltage V_{w2} gives the ions too much energy when crossing into the bunching section in lower potential, causing a drop in transmission as the ions collide with the electrodes.

Figure 25 shows the transmission and average time of flight for ions reaching the first bunching section, with parameters other than V_{w2} and bunching section DC voltages being the same as in table 1. Most notably, the time of flight is reduced for steeper gradients, which can be useful when dealing with short lived nuclei. The drop in transmission can partly be due to the fact the buncher was optimised to work with a V_{w2} value of 4880 V. It is thus possible the transmission can be improved by adjusting the potential in the first bunching section to better receive the ions.

6.2.3 RF phase dependency of injection

In the optimised simulations, the ions were always initialised at time $t = 0$, meaning that the phase of the RF signal was always the same at the start, while in reality ions will be entering the buncher during all phases. Thus it needed to be checked, whether there is a dependence on the transmission of the device and the phase of the RF signal during injection.

As the period of a 500 kHz signal is 2 μs, the effect was examined by scanning the initial phase over one period in steps of 0,1 μs from 0 μs to 1.9 μs. The transmission of the buncher injection was consistently over 99 %, indicating no apparent relation between the injection transmission and the RF phase. There was no need to simulate further segments, as the ToF spread of the ions at the end of the injection simulation was already longer than multiple periods. While the phase of the RF didn't appear to have any effect on the performance, according to the Mathieu parameters, its amplitude and frequency definitely have.

6.2.4 RF signal amplitude and frequency

The motion induced in the ions by the RF signal affect the properties of the extracted bunch. In this set of simulations, the amplitude and frequency of the signal in the second bunching section were scanned. The parameters were scanned individually, i.e. the voltage was kept constant while the amplitude was changed and vice versa. The ions of the optimised run in the first bunching section were used to initialise the ions in the scan.

The ToF and energy widths, and transmission of the bunch is shown in figures 26 and 27. It can be seen that for the right choice of RF amplitude and frequency, and thus the Mathieu parameters, the ToF and energy spread of the bunch can be minimised. The transmission stays nearly constant until an unstable region in the stability diagram is reached. A better picture of the stable region could be formed by scanning a larger frequency-amplitude phase space, but simulating a reasonable number of ions to obtain proper results would require a lot of time.

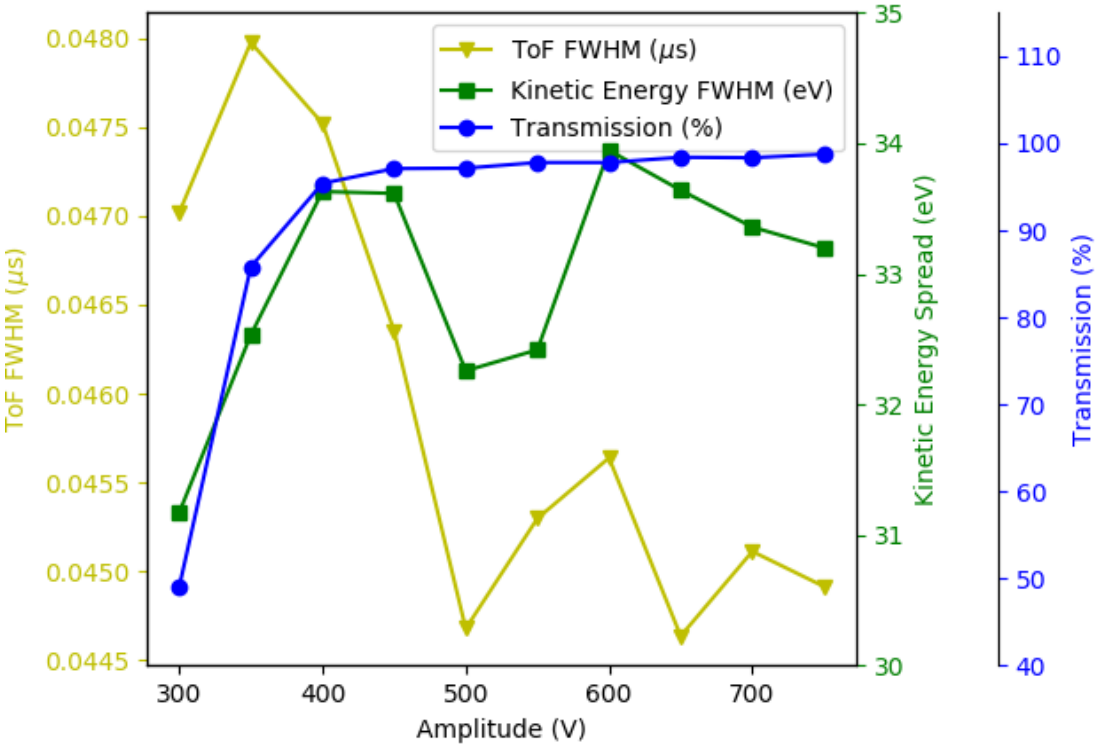

Figure 26. The transmission, and ToF and energy FWHM of a bunch with different RF amplitudes.

6.2.5 Cooling time

The temperature of the ion cloud plays a role in the properties of the extracted bunch. To study the relation, the time before extraction from the second bunching section was scanned. For these simulations, the ions of the optimised run in the first bunching section were used to initialise the ions.

The ToF and energy widths, and the transmission of the bunch just before extraction can be seen in figure 28. Predictably, longer time before extraction leads to lower temperatures of the bunch, albeit with diminishing returns. The reduced temperature is then seen in reduced ToF and energy spread. With a cooling time of 300 μs or less, the ions have too much radial motion to make it through the extraction aperture. Similarly to cooling time, the amount of interaction between the ions and the gas can be changed by altering the gas pressure.

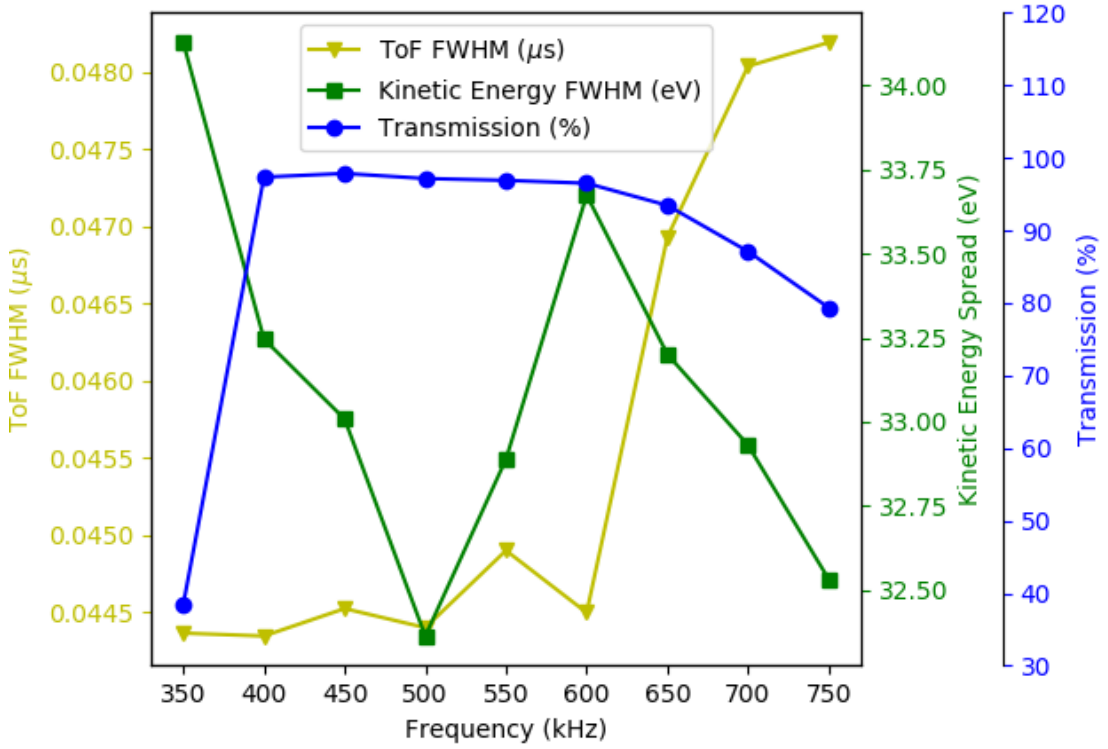

Figure 27. The transmission, and ToF and energy FWHM of a bunch with different RF frequencies.

6.2.6 Gas pressure

As the gas pressure in the second bunching section affects the quality of the bunches, simulations using different gas pressures in the second bunching section while keeping a constant cooling time were done. For these simulations, ions of the optimised run cooled in the first bunching section were used. The results of the simulations are shown in figure 29.

With lower pressures the ions didn't have enough time to cool down after the transfer from the first bunching section to the second, leading to large time-of-flight and energy spreads. In addition to the large radial motion, axially confining the ions in the second bunching section became harder, causing a large decrease in transmission. While the higher pressures allowed for sufficient cooling, the ion-gas collisions during extraction caused the distributions to become skewed, increasing the widths. It seems that a fine control of the pressure would be desired. In practice, changing the pressure of just the one section could possibly be done by adding a

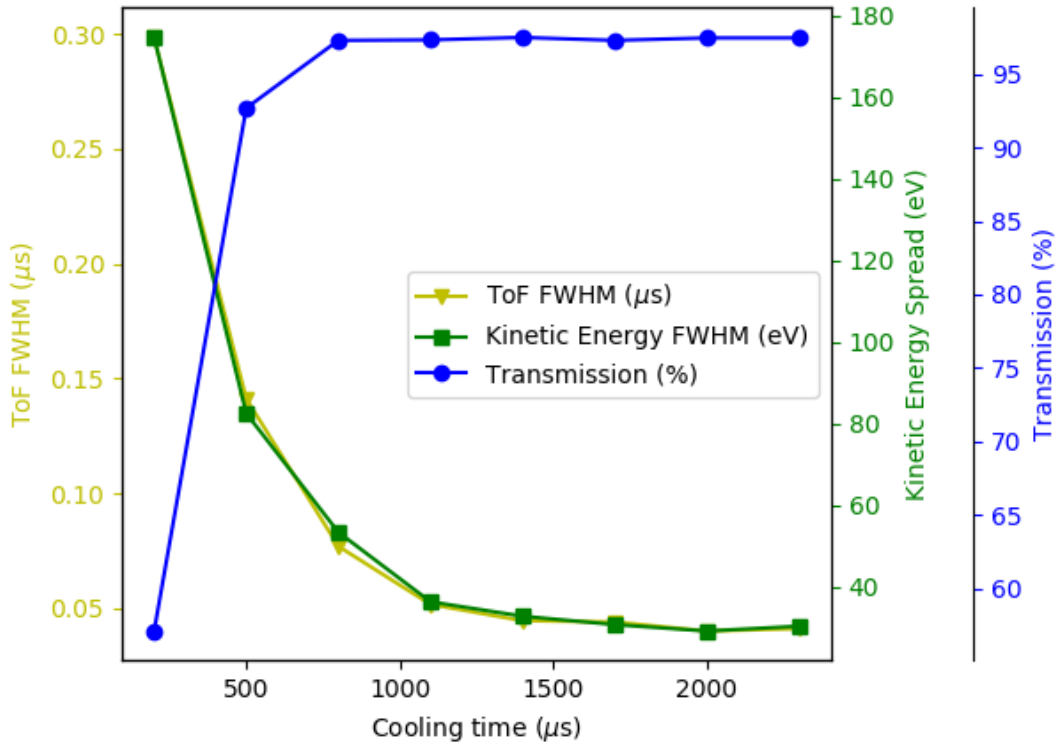

Figure 28. The transmission, and ToF and energy FWHM of a bunch with different cooling times before extraction from the second bunching section, i.e. the time after the "transfer" phase in table 1.

valve to the section, from which gas could be let in or pumped out. Just as the cooling time and the pressure could be used to control the amount of thermal motion the ions have before extraction, the depth of the axial potential well defines how far away from the axial minimum the thermalised ions can travel.

6.2.7 Depth of the bunching section potential well

To observe the effect of the potential well depth before extraction on the resulting bunch, the ions of the optimised run in the first bunching section were initialised and the DC component of the middle ring of electrodes in the second bunching section, V_{s4} in table 1, was changed. The widths of the resulting bunch and the transmission can be seen in figure 30.

Deepening the well reduces distance the ions travel from the minimum, reducing the energy spread the ions receive during extraction. If no other parameters are

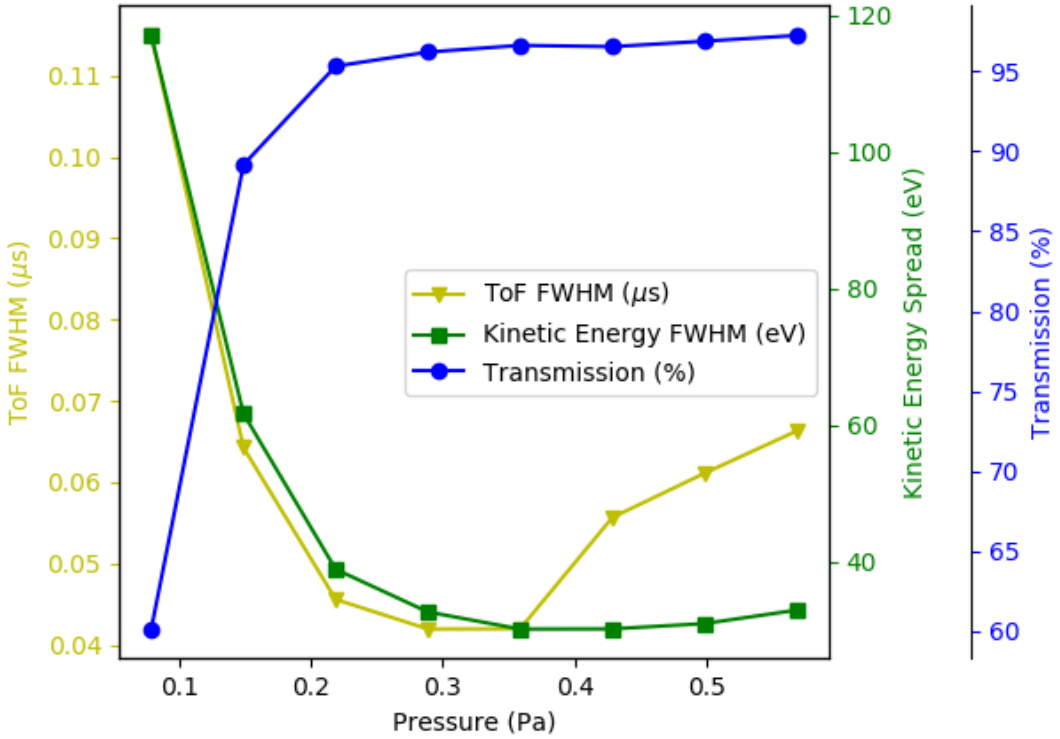

Figure 29. The transmission, and ToF and energy FWHM of a bunch with different pressures in the second bunching section, p_4 in table 1.

adjusted, the amount of induced motion before extraction can increase due to changing Mathieu parameters, reducing transmission. Although the depth of the potential well defines the distance the ions can move from the axial minimum, the potential gradient during extraction defines the energy difference between the ions furthest on the opposite sides of the minimum receive.

6.2.8 Extraction potential

The gradient in the second bunching section during extraction affects the width of the bunch as it changes the position of the time-focus plane. To observe the effect, the V_6, V_7 and V_8 were changed as shown in table 2. For these simulations, the ions of the optimised run in the first bunching section were used. The resulting temporal and energy widths are shown in figure 31.

From the figure, it can be seen that using the values in table 1 strike a good balance between a short temporal spread at the end of the simulated volume and

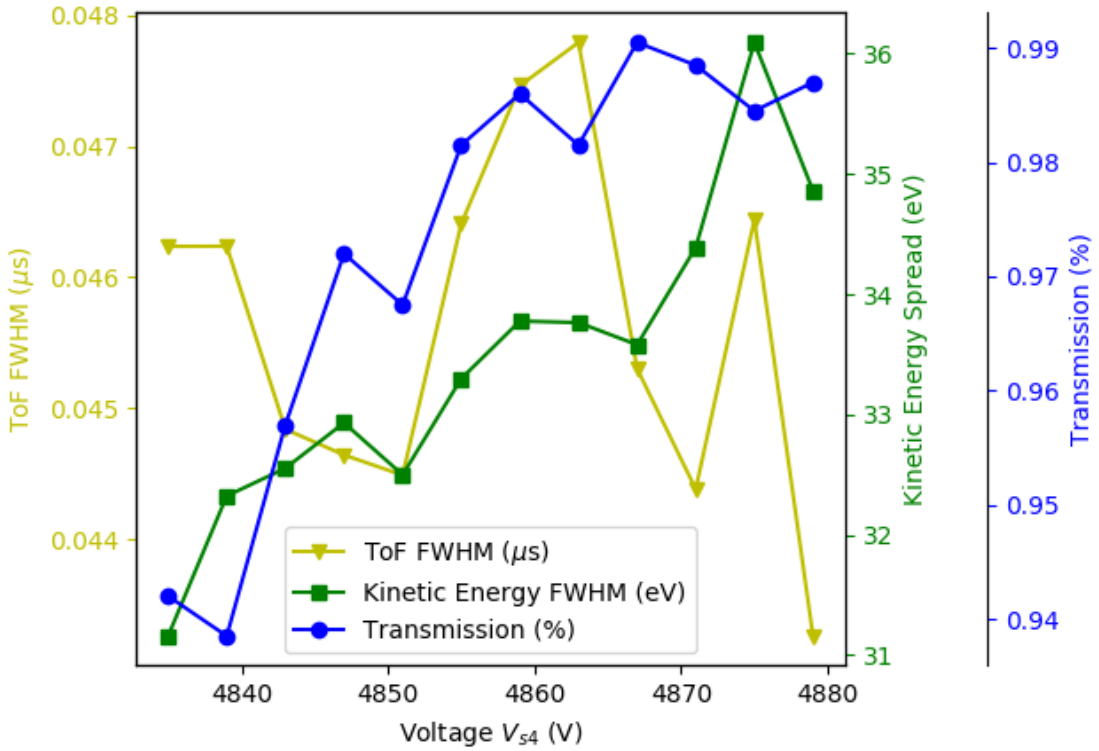

Figure 30. The transmission, ToF and energy FWHM of a bunch using different voltages V_{s4}, i.e. the depth of the potential well in the second bunching section, before extraction.

small energy distribution, as the width of the energy distribution continues to grow with increasing extraction potential gradient. The transmission stays consistent with a wide range of extraction potentials.

6.2.9 Ions of different masses

In the previous simulations, only ions of mass 100 u have been considered. For a buncher to be a worthwhile addition to a beamline, it needs to be able to operate on ions of different masses. To test the capabilities of the design, ions of masses of 20 u and 200 u were simulated starting from the injection. Mostly the operational parameters in table 1 could be used, but some parameters, namely the RF amplitude and frequency, had to be adjusted. The adjusted parameters are shown in table 3.

Optimising for short temporal spread, the 20 u ion bunch had a width of 14 ns and 30 eV, with a transmission of 66 %. The 200 u ion bunch had a width of 73 ns

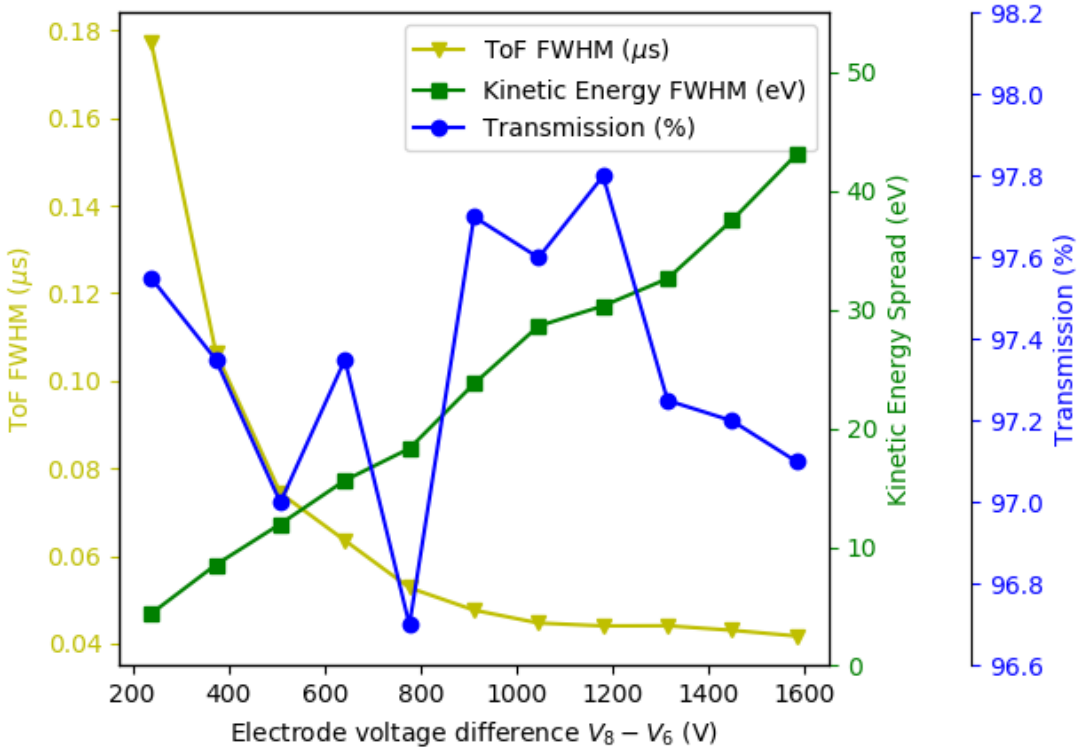

Figure 31. The transmission, and ToF and energy FWHM of a bunch using different extraction potentials. The exact electrode potentials can be found in table 2.

and 47 eV, with a transmission of 84 %. From the results, it can be seen that the buncher can be used for a variety of masses, although the transmission was noticeably worse. In these simulations, most ions were lost during extraction, as the extracted ions collided with the plate electrodes following the bunching section, V_7 and V_8 in figure 21. In these simulations, the gas pressure was not altered, which could result in better performance. It is likely that further adjustment of other operational parameters could also improve the results.

From the Mathieu parameters (15), it is possible to see that the parameters depend on the mass and charge of the ions as

$$a_i \propto \frac{q}{m} \quad q_i \propto \frac{q}{m}. \tag{29}$$

According to these mass simulations, if ions of mass 100 u were used, it would then be possible to bunch doubly charged ion, as the Mathieu parameters would be the

Table 2. In this table, the electrode voltages V_6. V_7 and V_8 used to evaluate different extraction potentials are presented. On each row is the set of voltages used in each run, with the results presented in figure 31. The parameters not shown in this table are the same as in table 1.

	Electrode voltages		
Run number	V_6	V_7	V_8
1	4964	4883	4725
2	5023	4877	4650
3	5083	4870	4575
4	5142	4864	4500
5	5201	4857	4425
6	5261	4851	4350
7	5320	4844	4275
8	5380	4838	4200
9	5439	4831	4125
10	5498	4825	4050
11	5558	4818	3975

Table 3. The operational parameters of the buncher, optimised for ions of different masses. The parameters not shown in this table are the same as in table 1. The parameters are indicated as (value for ion mass 20 u)/(value for ion mass 200 u).

	Operation phase		
Parameter	**Accumulation**	**Transfer**	**Extraction**
Phase start time, t	0 μs	8100 μs	9600 μs
RF rods, AC amplitude, V_{AC}	300 V/300 V	-	-
RF rods, frequency, f_{AC}	800 Hz/250 Hz	-	-
1st bunching plate, V_4	4891 V	4892 V/4910 V	4891 V
2nd bunching plate, V_5	4893 V	4885,5 V/4884,5 V	4893 V
3rd bunching plate, V_6	4900 V	4881,5 V/4884,5 V	5100 V/5400 V
4th segment ring, DC, V_{s3}	4881.5 V	-	-
5th segment ring, DC, V_{s4}	4860 V	-	-
6th segment ring, DC, V_{s5}	4874.2 V	-	-
End plate, V_7	4898 V	4898 V	4600 V/4800 V
Skimmer plate, V_8	4200 V/4500 V	-	-
1st extraction lens, V_9	4366 V/4166 V	-	-

same as with singly charged mass 50 u ions. Finally, the space charge effect was considered by taking the Coulomb repulsion into account.

6.2.10 Coulomb repulsion, space charge effects

Under the assumption that the beam currents will be low enough for the space charge effect to limit the performance, the Coulomb repulsion was not considered in these simulations. To asses the validity of this assumption, a beam of 400 pA was simulated flying through the buncher starting from the injection.

To create the beam, 225 particles were simulated, each starting 4 μs apart, where each of the ions represent 10000 actual ions. This creates an apparent current of 400 pA. The temporal spread of the extracted bunch was 79 ns and the energy width 50 eV, with transmission being 31,1 %. These values are somewhat worse than the results without the repulsion with the optimised parameters in chapter 6.2.1, especially the transmission. Most particles were lost in the transfer from the first to the second bunching section, which seems reasonable as the ions after accumulation are closer together than in a moving beam, increasing the space charge effect, and the ions have to pass through a small aperture. Due to the small number of simulated particles, the temporal and energy spreads were obtained using the equation 9 and thus the values might not be directly comparable with the other results.

This assessment needs to be taken with a grain of salt, as SIMION is not well suited to handle a large number of ion-ion interactions, or ions that move close to electrodes. As the simulations were done using the operational parameters not taking the repulsion into account, it is possible that better results could be obtained after some adjustment.

7 Conclusions

In this work, the geometry for an RFQ cooler-buncher and its injection and extraction optics were designed. The ion trajectory simulation software SIMION was used to evaluate the design's performance and to find such operational parameters for the buncher, that bunches with short temporal spread and small energy distribution could be created. In addition, the transmission had to be as high as possible and the transverse emittance small. The design presented in this work was the culmination of tens of iterations and it proved to be successful. A new method of using triangular wedge electrodes to create the gradient transferring the ions through the buncher was also tested and found to work well. The actual buncher can thus be constructed based on this work.

Using the operational parameters optimised for short temporal spread, bunches with 5 keV kinetic energy, 43 ns temporal spread and 30 eV energy width were obtained with 96 % transmission and 9 π·mm·mrad transverse emittance. With the parameters optimised for small energy spread, a spread of 0,78 eV could be reached with a temporal width of 1,1 μs. The injected beam consisting of singly charged mass 100 u ions had an emittance of 17 π·mm·mrad and kinetic energy of 5 keV. The design was also found to work well for beams consisting of mass 20 u and 200 u ions though with further optimisations the transmission is expected to improve.

Compared to other cooler-bunchers currently in use, apart from the higher transmission, this design performs quite similarly. For example, the cooler-buncher at JYFL can be operated in two different bunching modes, where one mode is capable of producing bunches with $<$100 ns temporal spread and $>$5 eV energy spread, and the other mode bunches with $\approx$10 μs temporal spread and $<$1 eV energy spread [39]. With the ISCOOL at ISOLDE, bunches with $<$5 μs temporal spread and $<$1 eV energy spread are achieved [1, 40]. For both devices, the transmission in shoot through mode, i.e. if the ions are not bunched, is around 75 % [1, 37, 40]. The transmission of 96 % achieved in this work for bunched ions would thus be a significant improvement if it also holds for the actual device. The design was able to cool and bunch the ions in just under 10 ms, which is in the typical range for such a

device [3, 25, 37], although a wide range of cooling times are employed.

In addition to finding the optimal operational parameters, simulations were also done to evaluate the effect of some key parameters on the quality of the bunched beam. As expected, the gas pressure, and electric potential during extraction had the clearest impact on the resulting spreads. When testing the actual device, it is thus important to carefully choose the values for these parameters. Particularly, the potential gradient during extraction needs to be adjusted to set the time-focus plane to a suitable location.

More accurate simulations could be achieved by using a denser point grid to model the electric field in SIMION, which would require a large amount of memory, and using more accurate parameters for the gas model. While the assumptions used in the gas model hold quite well [17, 28], in a future study, the pressure gradient throughout the volume could be modelled more accurately. Additionally, it would be interesting to better study the space charge effect on the accumulated ions.

Finally for suggestions on the actual device, making the pressure in the second bunching section controllable could lead to better quality bunches, as it can difficult to accurately adjust the pressure of the section simply by changing the pressure in the main RFQ section. Similarly, making the amplitude and frequency of the RF signal in the second bunching section controllable separately from the main RFQ section could be beneficial, as the accumulation potential shape in the second section can differ from the potential in the first bunching section, resulting in different Mathieu parameters.

References

[1] R. Catherall et al. “The ISOLDE facility”. In: 44.9 (Aug. 2017), p. 094002. DOI: 10.1088/1361-6471/aa7eba.

[2] R. Neugart et al. “Collinear laser spectroscopy at ISOLDE: new methods and highlights”. In: 44.6 (Apr. 2017), p. 064002. DOI: 10.1088/1361-6471/aa6642.

[3] B. Barquest et al. “RFQ beam cooler and buncher for collinear laser spectroscopy of rare isotopes”. In: 866 (Sept. 2017), pp. 18–28. DOI: 10.1016/j.nima.2017.05.036.

[4] R. Ringle, S. Schwarz, and G. Bollen. “Penning trap mass spectrometry of rare isotopes produced via projectile fragmentation at the LEBIT facility”. In: *International Journal of Mass Spectrometry* 349-350 (Sept. 2013), pp. 87–93. DOI: 10.1016/j.ijms.2013.04.001.

[5] D. A. Nesterenko et al. “Study of radial motion phase advance during motion excitations in a Penning trap and accuracy of JYFLTRAP mass spectrometer”. In: 57.11 (Nov. 2021). DOI: 10.1140/epja/s10050-021-00608-3.

[6] IAEA. *Live Chart of Nuclides*. URL: https://www-nds.iaea.org/relnsd/vcharthtml/VChartHTML.html. (accessed: 26.10.2021).

[7] M. Winkler et al. “The status of the Super-FRS in-flight facility at FAIR”. In: 266.19-20 (Oct. 2008), pp. 4183–4187. DOI: 10.1016/j.nimb.2008.05.073.

[8] R. Ringle et al. “Precision mass measurements with LEBIT at MSU”. In: *International Journal of Mass Spectrometry* 251.2-3 (Apr. 2006), pp. 300–306. DOI: 10.1016/j.ijms.2006.02.011.

[9] A. Valverde et al. “A cooler-buncher for the N=126 factory at Argonne National Laboratory”. In: 463 (Jan. 2020), pp. 330–333. DOI: 10.1016/j.nimb.2019.04.070.

[10] A. Nieminen et al. “Beam cooler for low-energy radioactive ions”. In: 469.2 (Aug. 2001), pp. 244–253. DOI: 10.1016/s0168-9002(00)00750-6.

[11] I. Moore et al. “Towards commissioning the new IGISOL-4 facility”. In: 317 (Dec. 2013), pp. 208–213. DOI: 10.1016/j.nimb.2013.06.036.

[12] M. Durante et al. “All the fun of the FAIR: fundamental physics at the facility for antiproton and ion research”. In: 94.3 (Jan. 2019), p. 033001. DOI: 10.1088/1402-4896/aaf93f.

[13] FAIR. *Overview on FAIR*. URL: https://fair-center.eu/. (accessed: 26.10.2021).

[14] H. Fynbo, O. S. Kirseboom, and O. Tengblad. “ISOLDE decay station for decay studies of interest in astrophysics and exotic nuclei”. In: 44.4 (Mar. 2017), p. 044005. DOI: 10.1088/1361-6471/aa5e09.

[15] M. Ranjan et al. “Design, construction and cooling system performance of a prototype cryogenic stopping cell for the Super-FRS at FAIR”. In: 770 (Jan. 2015), pp. 87–97. DOI: 10.1016/j.nima.2014.09.075.

[16] R. D. Knight. *Physics for Scientists and Engineers: A Strategic Approach with Modern Physics, 4th Edition*. Pearson, 2017.

[17] I. P. Aliseda. “New developments on preparation of cooled and bunched radioactive ion beams at ISOL-facilities: The ISCOOL project and the rotating wall cooling”. PhD thesis. Universitat Politècnica de Catalunya, 2006.

[18] P. Dahl. “Electron and Ion Optics”. In: Elsevier, 1973, pp. 1–2. DOI: 10.1016/b978-0-12-200650-0.50004-0.

[19] G. Werth, V. N. Gheorghe, and F. G. Major. *Charged Particle Traps II*. Springer Berlin Heidelberg, 2009. DOI: 10.1007/978-3-540-92261-2.

[20] H. Okamoto, Y. Wada, and R. Takai. “Radio-frequency quadrupole trap as a tool for experimental beam physics”. In: *Nuclear Instruments and Methods in Physics Research Section A: Accelerators, Spectrometers, Detectors and Associated Equipment* 485.3 (June 2002), pp. 244–254. DOI: 10.1016/s0168-9002(01)02139-8.

[21] T. Brunner et al. “TITAN’s digital RFQ ion beam cooler and buncher, operation and performance”. In: 676 (June 2012), pp. 32–43. DOI: 10.1016/j.nima.2012.02.004.

[22] M. Szilagyi. *Electron and Ion Optics*. Springer US, 1988. DOI: 10.1007/978-1-4613-0923-9.

[23] T. Kalvas. “Development and use of computational tools for modelling negative hydrogen ion source extraction systems”. PhD thesis. University of Jyväskylä, 2013.

[24] J. L. Wiza. “Microchannel plate detectors”. In: *Nuclear Instruments and Methods* 162.1-3 (June 1979), pp. 587–601. DOI: 10.1016/0029-554x(79)90734-1.

[25] S. Schwarz et al. “The LEBIT ion cooler and buncher”. In: *Nuclear Instruments and Methods in Physics Research Section A: Accelerators, Spectrometers, Detectors and Associated Equipment* 816 (Apr. 2016), pp. 131–141. DOI: 10.1016/j.nima.2016.01.078.

[26] F. Herfurth et al. “A linear radiofrequency ion trap for accumulation, bunching, and emittance improvement of radioactive ion beams”. In: *Nuclear Instruments and Methods in Physics Research Section A: Accelerators, Spectrometers, Detectors and Associated Equipment* 469.2 (Aug. 2001), pp. 254–275. DOI: 10.1016/s0168-9002(01)00168-1.

[27] E. W. Weisstein. *Gaussian Function*. URL: https://mathworld.wolfram.com/GaussianFunction.html. (accessed: 26.10.2021).

[28] L. Ding, M. Sudakov, and S. Kumashiro. “A simulation study of the digital ion trap mass spectrometer”. In: *International Journal of Mass Spectrometry* 221.2 (Nov. 2002), pp. 117–138. DOI: 10.1016/s1387-3806(02)00921-1.

[29] A. Reuben et al. “Ion trajectories in exactly determined quadrupole fields”. In: *International Journal of Mass Spectrometry and Ion Processes* 154.1-2 (May 1996), pp. 43–59. DOI: 10.1016/0168-1176(96)04374-1.

[30] J. Heinrich. “A Be+ Ion Trap for H+ 2 Spectroscopy”. PhD thesis. University of Sorbonne, 2018.

[31] C. Jesch. “The Multiple-Reflection Time-of-Flight Isobar Separator for TITAN and Direct Mass Measurements at the FRS Ion Catcher”. PhD thesis. University of Gießen, 2016.

[32] E. Haettner et al. “A versatile triple radiofrequency quadrupole system for cooling, mass separation and bunching of exotic nuclei”. In: *Nuclear Instruments and Methods in Physics Research Section A: Accelerators, Spectrome-*

ters, Detectors and Associated Equipment 880 (Feb. 2018), pp. 138–151. DOI: 10.1016/j.nima.2017.10.003.

[33] C. M. Lock and E. W. Dyer. "Simulation of ion trajectories through a high pressure radio frequency only quadrupole collision cell by SIMION 6.0". In: *Rapid Communications in Mass Spectrometry* 13.5 (Mar. 1999), pp. 422–431. DOI: 10.1002/(sici)1097-0231(19990315)13:5<422::aid-rcm503>3.0.co;2-m.

[34] L. Adaptas Solutions. *SIMION 2020 Supplemental Documentation*. URL: https://simion.com/info/. (accessed: 26.10.2021).

[35] M. E. J. Newman. *Computational physics*. North Charleston, SC: Createspace, 2013. ISBN: 1480145513.

[36] M. Schuh. "Simulations of the image chargeeffect in high-precision Penningtraps and the new IGISOL ionbuncher". PhD thesis. Ruperto-Carola-University of Heidelberg, 2019.

[37] R. de Groote et al. "Upgrades to the collinear laser spectroscopy experiment at the IGISOL". In: 463 (Jan. 2020), pp. 437–440. DOI: 10.1016/j.nimb.2019.04.028.

[38] M. Mantina et al. "Consistent van der Waals Radii for the Whole Main Group". In: 113.19 (Apr. 2009), pp. 5806–5812. DOI: 10.1021/jp8111556.

[39] H. Penttilä et al. "Radioactive ion beam manipulation at the IGISOL-4 facility". In: 239 (2020). Ed. by Z. Ge et al., p. 17002. DOI: 10.1051/epjconf/202023917002.

[40] C. Ricketts et al. "A compact linear Paul trap cooler buncher for CRIS". In: 463 (Jan. 2020), pp. 375–377. DOI: 10.1016/j.nimb.2019.04.054.

[41] G. Araneda. "Experiments with single photons emitted by single atoms". en. In: (2019). DOI: 10.13140/RG.2.2.33220.17288.

A Preparing the Inventor geometry for use in SIMION

In order to use the geometry designed in Autodesk Inventor in SIMION, the geometry data must first be converted to a point grid used by SIMION and the electric potential in the volume must be calculated. In short, to get the geometry into SIMION, first the Inventor assembly must be exported from the program using the "export/CAD format" option and selecting the stl format. Then the geometry in the stl files can be converted to a point grid, stored in a PA file, used by SIMION with the SLTools program. Finally the point grid can be loaded in SIMION and the potential must be calculated using the "refine" option on the main menu, after which the geometry is ready for use. What follows is a more complete explanation on the possible settings in this process.

When exporting an assembly from Inventor, a range of options can be set. The settings used in this work are shown in 32. On the top are the settings for the export format. Choosing "binary" instead of "ASCII" results in smaller sized files, but the files are intelligible to a human. As the files are not meant to be read, this is not an issue and the "binary" format is used. Additionally, the units used and the file structure of the exported files can be chosen. The "units" setting should be the same as the unit setting of the assembly, as otherwise the measures in SIMION will be different from those in Inventor. Of course, using the wrong setting is not catastrophic, but it will make analysing the results harder. The "structure" setting on the other hand must be on the "one file per part instance" setting, the other option being "one file", as SIMION sets the voltages of the electrodes on a per file basis. The "one file" setting would result in every electrode having the same voltage.

In stl format, the surface of the part is approximated with triangles. The resolution options define how many and how large triangles are used. For "surface deviation" and "normal deviation" lower values try to follow the surface more closely, resulting in more and smaller triangles. Exporting with better resolution results in larger file sizes, but the files are not typically large enough for the size to be an issue, and so

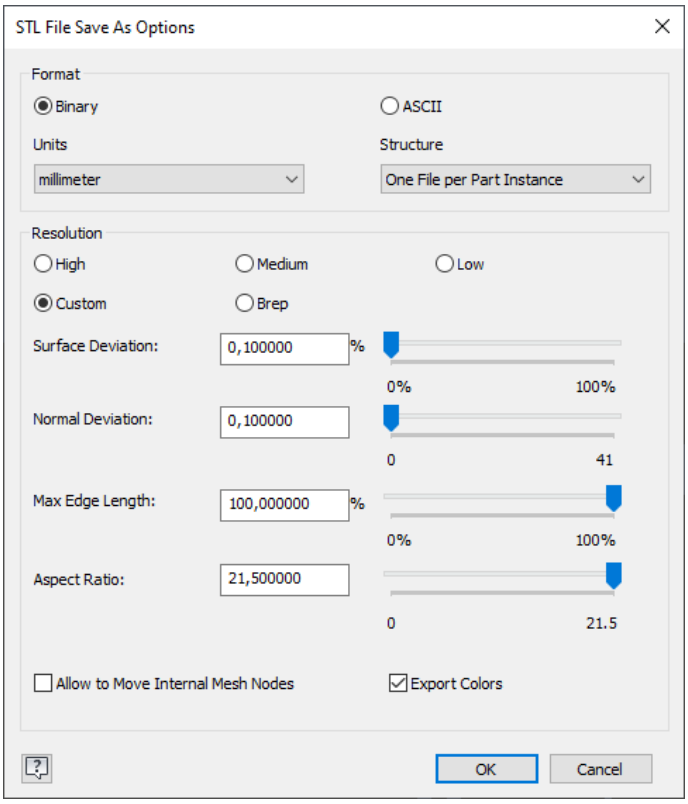

Figure 32. The export settings used in Autodesk Inventor.

the best possible settings were used. However, the default point grid in SIMION is often too sparse to take full advantage of the available resolution.

For SIMION to use the geometry, the stl files must be converted into PA files containing the point grid for the potential of each electrode. SLTools takes the multiple stl files exported from Inventor and outputs a single PA file that contains the point grid consisting of empty points and electrode points. To convert the stl files, the "STL -> PA" option in the sidebar must be chosen. The stl files to be converted must all have the same name ending with a different number that is greater than zero. When converting the geometry, some settings can be change to suit the application, with typical settings used in this work shown in figure 33.

In the "input file" field, one of the stl files can be selected. Replacing the number at the end of the filename with a % sign converts all stl files with the same name in the same folder, which is usually the desired outcome. Only the region and parts inside the rectangle defined by the "region min/max point" options are converted. The "region rotate" can be used to rotate the selected region in right angles. This can be used to make working with the device in SIMION more intuitive for the user,

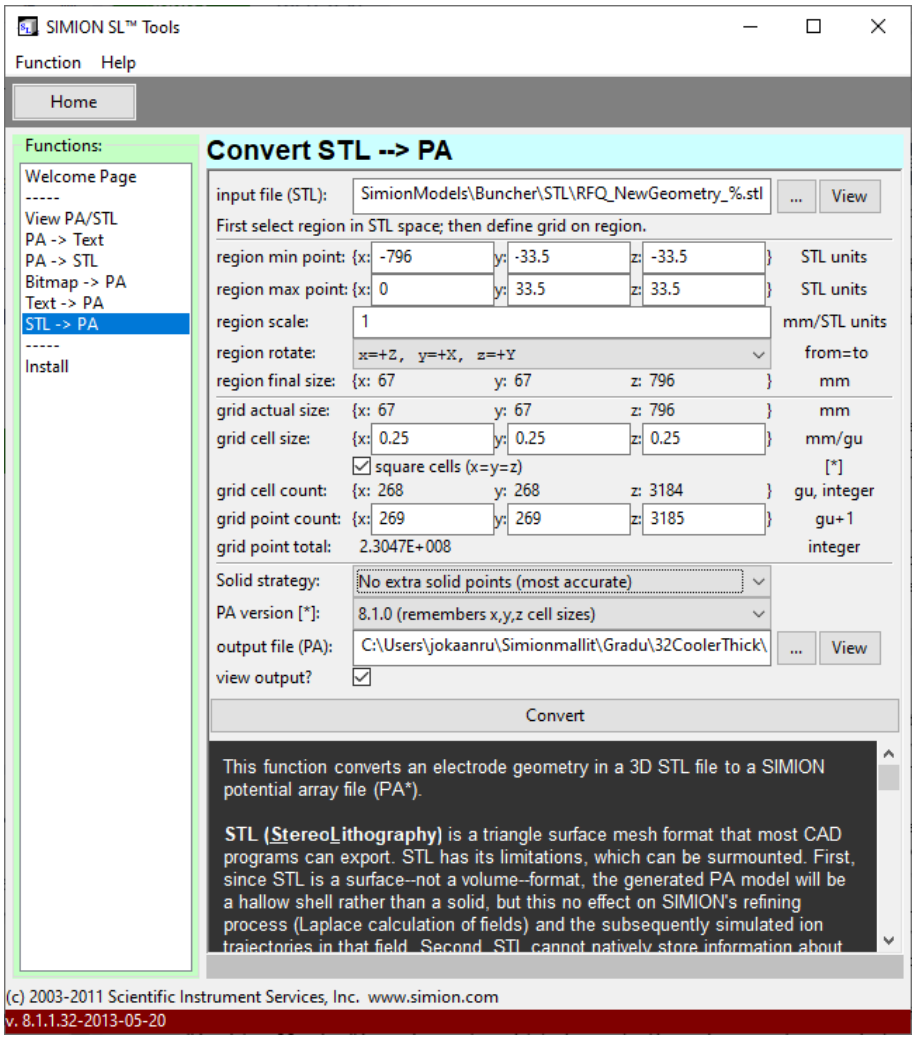

Figure 33. Typical settings in the SLTools program when converting the stl-files exported from Inventor to pa-files used by SIMION.

but it doesn't affect the quality of the simulation. The "region scale" option can be used to uniformly scale the x, y and z dimensions of the files, which might be useful if, for example, the dimensions of the stl files don't match the dimensions the parts have in Inventor. If the files were exported correctly from Inventor, the values should match and this option can be set to 1.

In the lower section of the settings, the width of each grid unit in millimetres can be set using the "grid cell size" option. The width in each direction can be set independently, but as this was not found to be useful in this work, a cubic grid was used. Of the settings available in this program, the density of the grid points have the greatest impact on the quality of the simulations, but also on the requirements

of the computer, the reason for which was explained in the section 5.1. In this work, grid densities of 0,3 mm/grid unit (gu), 0,33 mm/gg, 0,2 mm/gu and 0,25 mm/gu were used for the injection, main RFQ, first bunching, and bunching section and extraction optics respectively.

Finally, the way the grid points are placed on the surfaces is set with the "solid strategy" option and the "PA version" can be used to select the encoding of the .PA file created by the program. The "no extra points" "solid strategy" option is used in this work, as the surfaces of the electrodes more closely follow the surfaces in the stl files, and the option doesn't appear to have a downside. Also, the latest PA version is used.

After converting the model, it is possible to define the symmetry present in the model using SIMION. The available symmetries are planar and cylindrical. In this work, the planar symmetry option was used occasionally, as this makes it possible to import only one quadrant of the transverse plane of the buncher and SIMION creates the rest by mirroring the quadrant. This improves the performance of the simulation and cuts the memory usage of the program by four, as also the electric fields are symmetric and as such the three other quadrants don't need to be kept in memory. Unfortunately, the arrangement of the wedges in the main RFQ section of the buncher is symmetric about a point, and as such planar symmetry couldn't be used in the models where the main RFQ was present.

Before simulations can be performed, a few preparatory steps need to be taken in SIMION. First, on the front page of SIMION, the created PA file has to be loaded. Next the optional step of applying the symmetries must be taken by going to the "set params..." page in the "modify" option. Then the electric potential need to be calculated by going to the "refine" page and clicking "refine". The most important option on the page is the "convergence objective", which dictates how accurate the final potentials are, with lower value resulting in more accurate results. Using lower values can increase the time it takes to refine, but not by too much. The settings used in this work can be seen in 34.

For each stl file, refining creates a new PAx file, where the x is replaced with the number at the end of the stl file name. Each PAx file contains the electric potential of the respective electrode. After the refining is complete, the model can be opened by loading the .PA0 file and clicking "view/load workbench". Finally, before starting a simulation, the model must be saved using the "save..." button on the "workbench"

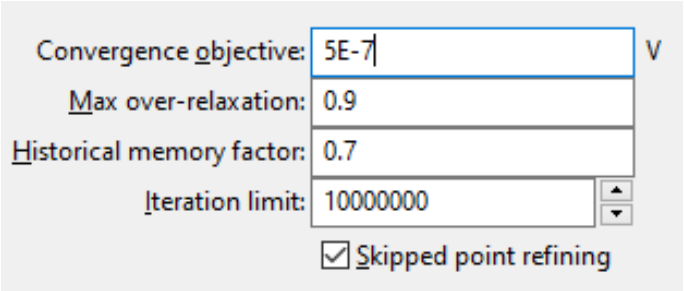

Figure 34. The settings used for refining the PA# file.

tab. Saving the model creates an iob file that contains some information about the model, and .fly2 and .rec files, that contain the ion settings and data recording settings. The model can also be loaded by clicking the "view/load workbench" button and selecting the iob file, if it already exists. After opening the workbench, if only static voltages are needed, the "fast adjust voltage" page in the "PAs" tab can be used to set the voltages, but if alternating voltages or voltage switching is needed, the "use program" box in the "particles" tab must be checked. This creates a new lua file that can be used to control the simulation. In order for the user program to work, the lua file and the iob file must have the same name.